npj | vaccines

Article

Published in partnership with the Sealy Institute for Vaccine Sciences

https://doi.org/10.1038/s41541-024-00942-9

A multi-targeting immunotherapy ameliorates multiple facets of Alzheimer's disease in 3xTg mice

Xuejian Feng[1], Yunyu Hou[1], Jiaxin Liu[1], Fei Yan[1], Mingrui Dai[1], Mo Chen[1], Jianan Wang[2], Jie Li[3], Zhenjiang Liu[1,4], Dong Sun[1,4], Yong Zhang[1,4], Xianghui Yu[1,4], Wei Kong[1,4] ✉ & Hui Wu[1,4] ✉

Alzheimer's disease (AD) is an intricate disorder involving amyloid deposits, neurofibrillary tangles, and chronic neuroinflammation. Though current Aβ-directed immunotherapies effectively eliminate amyloid plaques, their limited clinical benefits and notable safety concerns arise from overlooking two other neglected neurodegenerative features. Compelling evidence highlights synergistic cooperation between Aβ and tau, underscoring the imperative need to develop combinational therapies to target the diverse pathologies of AD. In this study, we present a dual AD vaccine combining Aβ and pTau vaccines, eliciting robust and enduring antibody responses against pathological Aβ and pTau in 3xTg transgenic mice. It significantly eradicated Aβ plaques and pTau tangles, suppressed neuroinflammatory factors, and markedly enhancing cognitive abilities in 3xTg mice. Mechanistically, peripheral antibodies penetrated the brain, recognizing and inhibiting Aβ and pTau aggregation, thereby reducing their cytotoxicity. In summary, this innovative multi-targeting immunotherapy remarkably ameliorates diverse AD pathologies, demonstrating maximum benefits in slowing the clinical progression of AD.

Alzheimer's disease (AD) is a heterogeneous neurodegenerative disorder characterized by multiple pathological features in the brain, such as extracellular senile plaques composed of β-amyloid (Aβ), intracellular neurofibrillary tangles (NFT) of hyperphosphorylated tau, activated microglia, and astrocytes, which lead to chronic neuroinflammation, synaptic dysfunction, neuronal loss, and cerebral atrophy[1]. Due to the intricacies of this disorder, current efforts to slow down AD's clinical progression have been largely unsuccessful.

Immunotherapy has emerged as a promising strategy in disease-modifying therapies (DMTs), aiming to directly eliminate the pathological factors in AD. Over the past decades, Aβ has been the primary target of AD immunotherapeutic strategies[2]. Recent clinical studies, particularly those utilizing Aβ-directed antibodies such as Lecanemab and Donanemab, provide renewed optimism for slowing cognitive decline in early-stage AD patients through immunotherapeutic strategies[3,4]. However, high-dose anti-Aβ passive immunization, effectively eliminates cerebral amyloid plaques, and yields relatively modest clinical benefits and notable safety concerns. In contrast, active immunotherapy, being a more accessible and cost-effective strategy, triggers a long-term antibody response with less frequent, smaller-dose administration[5]. Currently, four candidate active immunotherapies targeting Aβ are undergoing clinical trials, namely ALZ-101, ABvac 40, ACI-24, and UB-311[6]. UB-311, a synthetic peptide-based active immunotherapy targeting Aβ1-14, demonstrated safety and elicited robust Aβ antibodies in the majority of AD patients in its phase 2a clinical trial[7]. Although participants treated with UB-311 displayed a slight decrease in cortical amyloid PET burden and delayed cognitive decline, further investigation on a larger sample population is necessary to establish its clinical benefit.

Beyond the well-documented Aβ plaques, neurofibrillary tangles (NFTs) accumulated by hyperphosphorylated tau (pTau) stand out as another critical neuropathological signature of AD[8]. The phosphorylation of tau at multiple sites, such as Ser202, Thr205, Ser396, and Ser404, significantly increases in AD patients[9]. This modification not only precipitates the formation of NFTs but also leads to axon degeneration and neuronal loss[10]. A wealth of evidence has shown that the pathological state of hyperphosphorylated tau correlates more closely with the extent of cognitive decline than Aβ levels, prompting researchers to pivot towards tau-centric strategies for AD therapy and AD treatment[11]. ACI-35 developed by

[1]National Engineering Laboratory for AIDS Vaccine, School of Life Sciences, Jilin University, Changchun, 130012, China. [2]Changchun BCHT Biotechnology, 1260 Huoju Road, Changchun High-tech Zone, Changchun, Jilin, China. [3]Department of Geriatrics, The First Hospital of Jilin University, Changchun, 130021 Jilin, P.R. China. [4]Key Laboratory for Molecular Enzymology and Engineering, The Ministry of Education, School of Life Sciences, Jilin University, Changchun, 130012, People's Republic of China. ✉e-mail: weikong@jlu.edu.cn; topwuhui@jlu.edu.cn

AC Immune, emerges as the pioneering and sole anti-pTau active vaccine in clinical trials[12]. It contains 16 copies of a synthetic tau fragment phosphorylated at residues Ser396/404 and embedded into a lipid bilayer, and has shown positive safety, tolerability, and high immunogenicity. Notably, it exhibits exceptional specificity for pathological tau, sparing non-phosphorylated tau. While ACI-35 has successfully completed the phase I clinical trial, with results eagerly anticipated, it underscores the necessity for further investigation to fully ascertain its efficacy and potential in AD treatment.

Beyond the accumulation of Aβ and pTau aggregates, the involvement of immune mediators such as microglia activation, reactive astrogliosis, and various proinflammatory cytokines have been shown to play crucial roles in the progression of AD[13]. Initially, resting microglia can be activated by Aβ aggregates, which trigger the phagocytosis of Aβ. This process, in turn, further increases microglial activation[14]. Prolonged microglial activation, however, eventually impairs its phagocytic function, leading to excessive release of proinflammatory cytokines and exacerbating neuronal damage[15]. Additionally, microglia can also engulf neurons or synapses containing tau, potentially disseminate tau pathology through the release of tau tangles in exosomes[16]. Similarly, reactive astrocytes also respond to Aβ aggregates, activating target genes to produce proinflammatory factors[17,18]. This intricate interplay highlights the significant role of neuroinflammation in AD, making it a focal point of therapeutic intervention research[19]. Aβ immunotherapy trials, such as Lecanemab and Donanemab, have not only demonstrated efficacy in clearing aggregated Aβ but also in reducing plasma GFAP levels, indicating a decrease in astrocyte activation. Despite these advancements, the function of AD-active immunotherapies in modulating neuroinflammation in the human AD brain remains to be fully understood, necessitating thorough investigation to uncover how these treatments may influence the neuroinflammatory landscape of AD.

More recently, accumulating evidence has highlighted Aβ-pTau interactions and their synergistic effects in AD progression[20]. These findings reveal that aggregated Aβ can accelerate the hyperphosphorylation of tau by enhancing CDK-5 and GSK-3β activity[21,22]. Furthermore, pTau is known to mediate Aβ toxicity by interacting with Fyn kinase through its projection domain[23]. The synergistic actions of Aβ and pTau are particularly harmful to microglia, astrocytes, and the integrity of the blood–brain barrier network during AD's pathological process[24]. Recent human postmortem data have demonstrated that Aβ plaques and tau tangles cooperatively precipitate cognitive decline in human AD, highlighting the cooperative nature of these proteins in driving the disease's progression[25–27]. This synergy suggests that treatments targeting only Aβ or tau might not fully address the complexity of AD pathology. Despite the growing understanding of this interplay, so far, there has been no investigation on the combinational vaccine targeting Aβ and pTau simultaneously. The potential effects of such a vaccine on Aβ and Tau pathology, neuroinflammation, and its role in cognitive improvement in AD mouse remain unclear. This gap underscores the need for comprehensive approaches that consider the multifaceted interactions driving AD, potentially offering more effective therapeutic strategies.

In response to the complex interplay between Aβ and hyperphosphorylated tau (pTau) in Alzheimer's disease (AD), we designed a combinational AD vaccine that includes an Aβ epitope vaccine and a hyperphosphorylated tau (pTau) vaccine. The Aβ vaccine, comprising three copies of Aβ1–6 inserted into three loops of the norovirus P particle, elicited high antibody titers against Aβ42, effectively reducing amyloid deposition and mitigating memory loss in APP/PS1 mice[28]. Similarly, the pTau vaccine, by linking the pTau peptide encompassing four phosphorylation sites (pTau202/pTau205/pTau396/pTau404) to the surface of P particles, generated robust antibodies against four pTau epitopes, significantly diminishing neurofibrillary tangle (NFT) deposition, and improving behavioral deficits in TauP301S mice[29]. In this study, the therapeutic effects of the combinational Aβ vaccine and pTau vaccine were thoroughly evaluated in 3xTg AD mice harboring both the Aβ and pTau pathologies. We demonstrated that the combinational AD vaccine can induce robust and sustained antibody responses against various toxic forms of Aβ and pTau in 3xTg mice brains, regardless of illness stages. The most striking finding was the vaccine's superior efficacy in ameliorating behavioral and cognitive deficits in the AD mice, outperforming the outcomes seen with each vaccine administered alone. Moreover, there was a pronounced attenuation of neuroinflammatory responses in the cerebral tissues of the immunized AD mice. To summarize, this innovative multi-targeting immunotherapy substantially mitigates the myriad of pathological manifestations inherent to AD, culminating in optimal cognitive restoration in 3xTg mice.

Results

Combination of Aβ and pTau vaccine induces robust and long-term antibody responses against pathological Aβ and tau in 3xTg mice

To formulate a potent combinational AD vaccine for optimal therapeutic outcomes, we isolated recombinant P particles-based Aβ1–6 vaccine from a prokaryotic expression system (Supplementary Fig. 1a–d) and conjugated the pTau peptide, encompassing four phosphorylation sites (pTau202/pTau205/pTau396/pTau404), to the surface of P particles (Supplementary Fig. 1e–h). The combinational vaccine consisted of a blend of Aβ and pTau vaccines, each prepared in an equal mass ratio with CpG oligonucleotide and ZMF59 oil-phase emulsifier.

To evaluate the immunogenicity and safety of this combinational vaccine, we immunized a group of C57BL/6 wild-type mice with the dual vaccine and compared the results with those from groups receiving either the Aβ or pTau vaccine alone. The co-administration with Aβ and pTau vaccines induced high-titer antibodies specific to Aβ and all pTau epitopes in the peptide (Supplementary Fig. 2a, b). In comparison to single vaccines, the dual vaccine generated similar levels of anti-Aβ antibodies but significantly higher concentrations of pTau202/pTau205/pTau404 antibodies. Further evaluation of Aβ or Tau-specific T cells following the final immunization confirmed the dual vaccine's safety profile. We observed no emergence of T-cell responses specific for Aβ or Tau (Supplementary Fig. S2c–e). Moreover, immunization with the dual vaccine led to robust activation of P particle-specific T cells, providing Th cell-mediated activation for anti-Aβ/pTau-specific B cells (Supplementary Fig. 2f). Taken together, the concurrent immunization with Aβ and pTau vaccine elicited robust humoral immunity against Aβ and pTau epitopes without inducing epitope-specific T-cell activation in wild-type mice.

Subsequently, the 3xTg mouse model, housing both Aβ plaques and NFT in the brain, was employed to investigate the immunogenicity and efficacy of the dual vaccine. This study divided the transgenic mice into two cohorts for vaccination with either the dual or single vaccine formulations, using a prime-boost strategy (Fig. 1a). The premorbid cohort underwent immunization prior to the manifestation of AD pathology at 3.5 months, whereas the onset cohort received treatment subsequent to AD onset at 6 months. In the premorbid cohort, following the fourth immunization, the dual vaccine elicited a pronounced and targeted antibody response against Aβ42 and the quartet of pTau epitopes, with antibody titers ranging from 158.60 to 224.47 μg/mL (Fig. 1b, d and Supplementary Fig. 3a, c). After booster immunization, Aβ and pTau antibody titers were markedly enhanced to approximately 409.18 μg/mL. By the age of 10.5 months, the antibody titers remained elevated at around 400 μg/mL, indicating a sustained therapeutic effect. In the onset cohort, dual vaccine-immunized mice generated robust antibodies against various antigens, including Aβ42, pTau202/205, pTau396, and pTau404 (Fig. 1f, h and Supplementary Fig. 3e, g) after four immunizations. However, the average concentrations of Aβ antibodies were significantly lower than those in mice immunized before AD onset. Despite this, the booster strategy successfully reinforced the pTau antibody response in mice treated after AD onset, with the final antibody level remaining at 400 μg/ml (Fig. 1h). In contrast, the Aβ antibody response in the onset group failed to be activated after the booster administration (Fig. 1f).

Notably, the dual vaccine produced comparable titers of anti-Aβ antibodies, yet yielded markedly elevated levels of pTau antibodies in comparison to those observed in mice treated with a single vaccine,

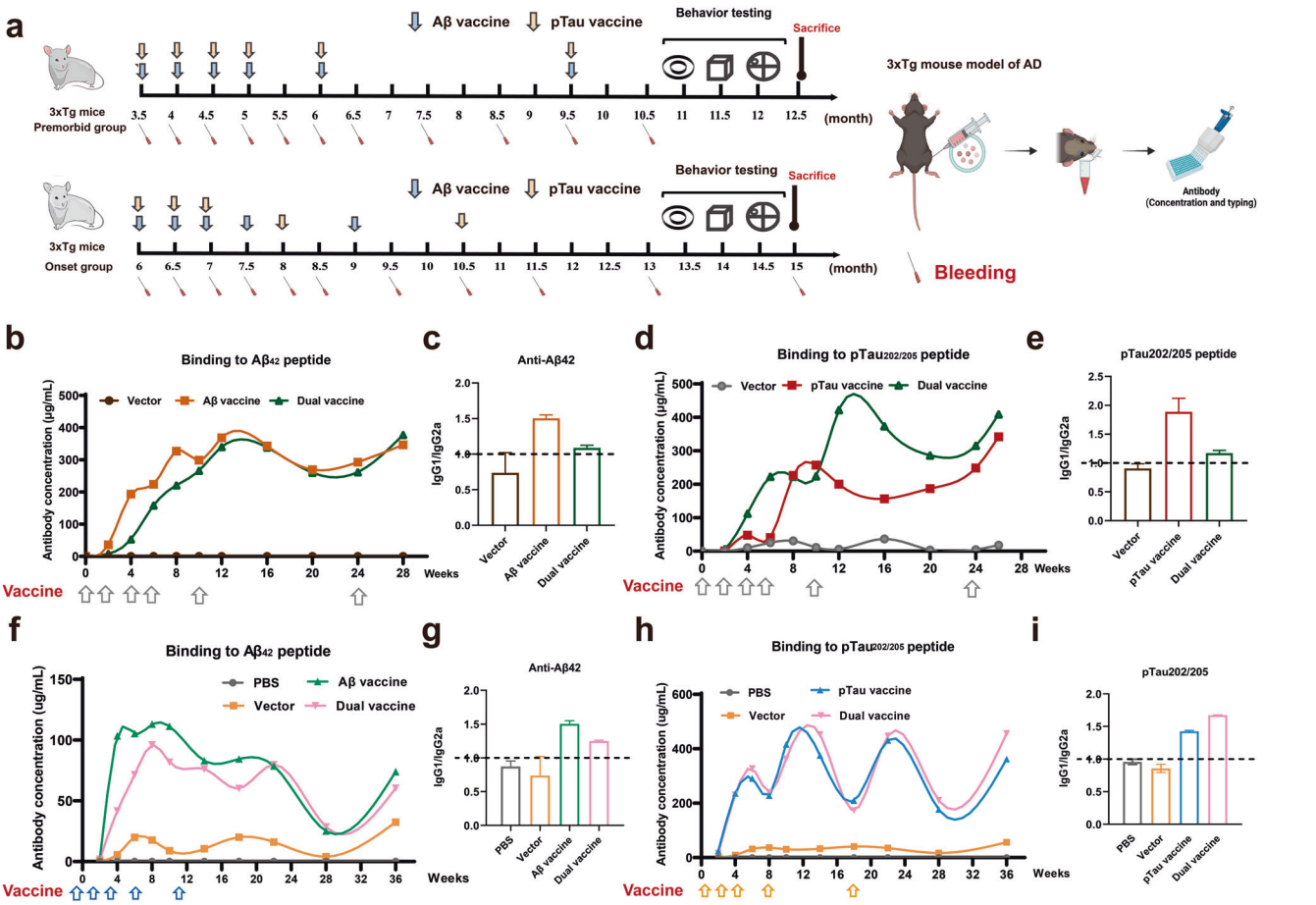

Fig. 1 | Immune response in vaccinated 3xTg mice. a Immunization and behavioral testing: Schematic outlining the immunization and behavioral testing procedures in the premorbid cohort (initiated at 3.5 months) and onset cohort (initiated at 6 months). **b**, **c** Aβ-specific antibodies (Premorbid Group): Concentration (**b**) and antibody typing (**c**) of Aβ-specific serum antibodies. **d**, **e** pTau202/205-specific antibodies (Premorbid Group): concentration (**d**) and antibody typing (**e**) of pTau202/205-specific serum antibodies. **f**, **g** Aβ-specific antibodies (Onset Group): Concentration (**f**) and antibody typing (**g**) of Aβ-specific serum antibodies. **h**, **i** pTau202/205-specific antibodies (Onset Group): Concentration (**h**) and antibody typing (**i**) of pTau202/205-specific serum antibodies. *Data presented as mean ± SEM. The arrows below the panel **b**, **d**, **f**, **h** indicate the immunization timepoint of the dual vaccine. (Created with Adobe Illustrator and BioRender.com).

regardless of age. As anticipated, these vaccines were immunospecific, as the administration of the Aβ vaccine alone did not induce anti-pTau antibodies and vice versa (data not shown). In addition, the antibodies induced by pTau vaccine or dual-targeting vaccine could not recognize non-phosphorylated Tau peptide, no matter from the premorbid (Supplementary Fig. 3i) or onset mice group (Supplementary Fig. 3k). We also noticed that the single vaccines and dual vaccine all induced antibodies against PP carrier protein in 3xTg mice, albeit to a lesser extent compared to the immune response specific for Aβ or pTau epitope (Fig. S3j, l). Furthermore, we characterized the types of humoral immune responses after vaccine administration through antibody typing analysis. Following vaccination, the ratio of IgG1 to IgG2a was higher than 1, indicating that the immune response induced by the PP-based combinational vaccine was skewed toward Th2 type (Fig. 1c, e, g, i and Supplementary Fig. 3b, d, f, h). In conclusion, combinational therapy with the mixture of Aβ and pTau vaccine successfully stimulates a potent and prolonged antibody response targeting various Aβ and pTau pathological epitopes simultaneously in 3xTg mice.

Dual vaccine mitigates Aβ and tau pathology in 3xTg mice from the premorbid cohort

The impact of the dual vaccine on AD pathology was assessed by comparing Aβ plaques and NFT deposition, as well as the levels of soluble and insoluble Aβ, and pTau protein in brain extracts of different vaccinated mice (Fig. 2a). When administered before AD onset, the dual vaccine significantly reduced Aβ load in the hippocampus and cortex of 3xTg mice, as analyzed by IHC staining (Fig. 2b). In contrast, mice treated with the single Aβ vaccine also exhibited a substantial reduction in Aβ deposition, however, the extent of Aβ clearance was discernibly inferior to that achieved by the dual vaccine (Fig. 2b). Furthermore, the relative area covered by Aβ plaques in the hippocampus and cortex of dual-vaccinated mice was reduced by 70.22 and 80.92%, respectively, compared to vector-vaccinated mice (Fig. 2c). Mice treated with the single Aβ vaccine also showed notable reductions in plaque area, 74.59% in the hippocampus and 60.25% in the cortex, though these were less effective than the dual vaccine's results. Notably, significant reductions in NFT containing different pTau epitopes were observed in mice treated with the dual vaccine, as well as those treated with the pTau single vaccine (Fig. 2e). Simila to the Aβ vaccine, the dual vaccine demonstrated a moderately superior effect in eliminating pTau tangles compared to the single vaccine. The relative areas covered by pTau202/205-, pTau396-, and pTau404-positive tau tangles in the hippocampus and cortex of dual vaccine-treated mice were all significantly decreased compared to vector-vaccinated mice (Fig. 2e, f, h, i, k, l). This investigation also highlighted that both single Aβ and pTau vaccines could individually reduce NFT accumulation and Aβ plaque formation, albeit to a lesser degree. This outcome underscores the synergistic interaction between Aβ and pTau pathologies in AD progression. Additionally, a clear trend towards a decrement in both soluble and insoluble Aβ42 was observed across all vaccinated mice (Fig. 2d and Supplementary Fig. 5a). Notably, dual vaccine treatment led to the lowest levels of soluble Aβ42 in the mouse

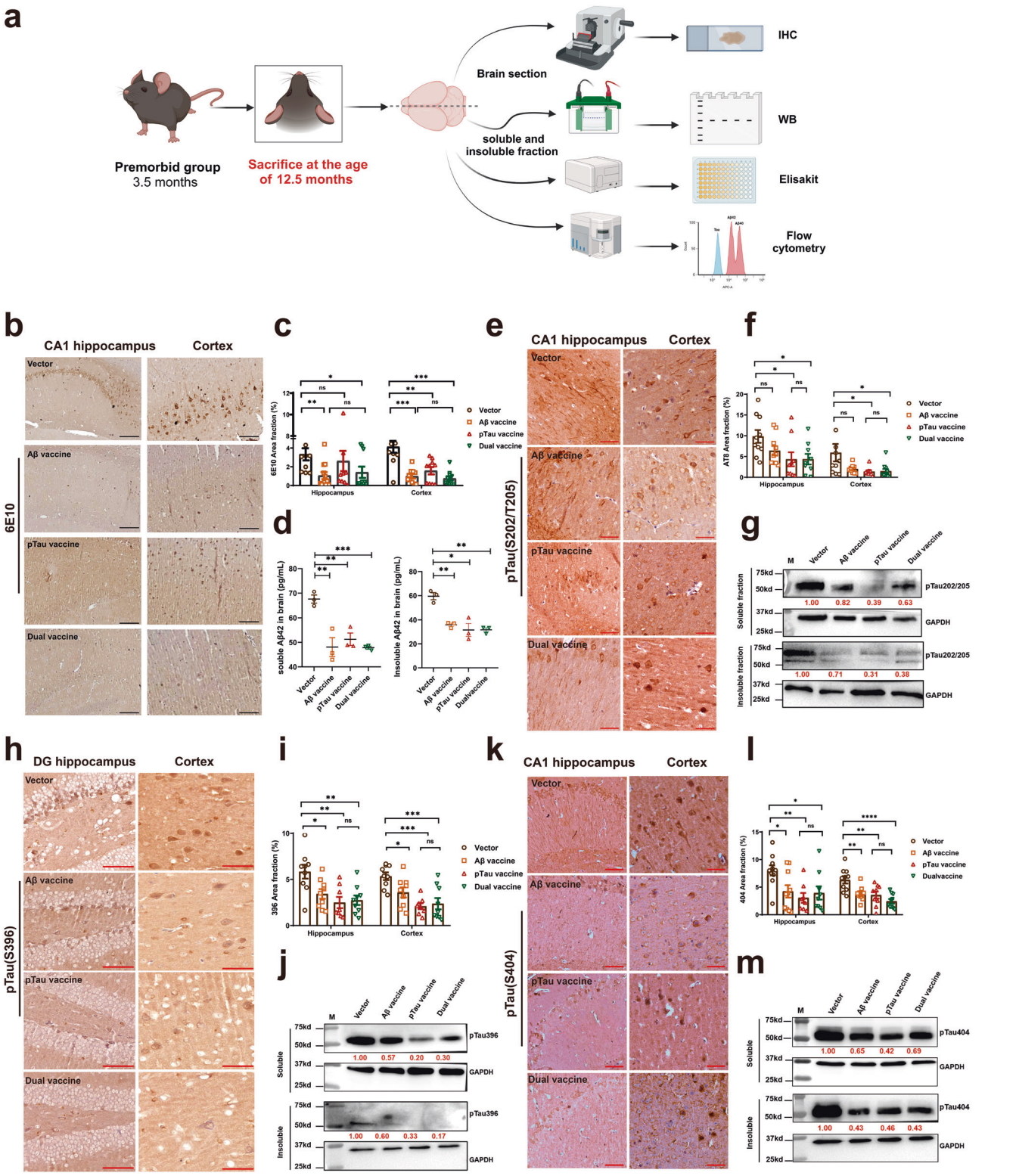

brain, thereby denoting the superior clearance efficiency of the dual vaccine formulation. Similarly, the combinational vaccine remarkably decreased the soluble and insoluble pTau levels in the brain lysates of 3xTg mice (Fig. 2g, j, m).

Furthermore, we analyzed the neuronal densities in the brains of vaccine-treated mice by IHC staining. In the premorbid cohort, we observed no difference in the total hippocampal NeuN area. However, the area of the neuronal (NeuN+) layer of the dentate gyrus granule cells was significantly increased in the dual vaccine-treated mice compared with the control and single vaccine groups, suggesting a neuroprotective effect of the dual vaccine (Supplementary Fig. 4a–c). However, in the onset group, the dual vaccine failed to attenuate neuronal death in the hippocampus of 3xTg mice (Supplementary Fig. 4d–f). Collectively, the antibody mixture elicited by the dual vaccine efficiently targeted the soluble and deposited Aβ and pTau pathological proteins simultaneously in the brains of AD mice, leading to the prevention of downstream neurodegeneration.

Fig. 2 | Changes in Aβ and tau pathology in premorbid 3xTg mice. a Methods for pathological evaluation: Outline of methods for evaluating mouse brain pathology after vaccine immunization. **b** Aβ Immunostaining: 6E10 immunostaining for Aβ burden in 3xTg mice brains. (Black scale bar: 100 μm). **c** Quantification of Aβ immunostaining: Quantification of 6E10 immunostaining in the hippocampal CA1 and cortex regions. **d** Aβ42 analysis: Aβ42 levels in soluble and insoluble brain homogenates by flow cytometry (The experimental samples are mixed samples (n = 9–10) and repeated three times). **e** pTau Immunostaining: AT8 immunostaining for phosphorylated-tau in 3xTg mice brains. (Red scale bar: 50 μm). **f** Quantification of pTau immunostaining: Quantification of AT8 immunostaining in the hippocampal CA1 and cortex regions (n = 9–10). **g** pTau202/205 analysis: pTau202/205 levels in soluble and insoluble brain homogenates by western blot (Mixed samples, n = 9–10). GAPDH served as the internal control. The relative content of each sample is marked with a red number. **h** PHF-13 Immunostaining: PHF-13 immunostaining for phosphorylated-tau in 3xTg mice brains. (Red scale bar: 50 μm). **i** Quantification of PHF-13 immunostaining: Quantification of PHF-13 immunostaining in the hippocampal DG and cortex regions (n = 9–10). **j** pTau396 analysis: pTau396 levels in soluble and insoluble brain homogenates by western blot (Mixed samples, n = 9–10). GAPDH served as the internal control. The relative content of each sample is marked with a red number. **k** Phospho-tau (Ser404) immunostaining: Immunostaining for phosphorylated-tau (Ser404) in 3xTg mice brains. (Red scale bar: 50 μm). **l** Quantification of phospho-tau (Ser404) immunostaining: Quantification of phospho-tau (Ser404) immunostaining in hippocampal CA1 and cortex regions (n = 9–10). **m** pTau404 analysis: pTau404 levels in soluble and insoluble brain homogenates by western blot (Mixed samples, n = 9–10). GAPDH served as the internal control. The relative content of each sample is marked with a red number. *Data presented as mean ± SEM. Multivariate ANOVA was employed when $p \le 0.05$. Bonferroni-corrected t-test was otherwise applied. Statistical significance denoted as $^{*}p < 0.05$, $^{**}p < 0.01$, $^{***}p < 0.001$; ns not significant. (Fig. 2a was created with BioRender.com).

Combinational vaccine improves motor function, recognition, and memory ability in 3xTg mice of the premorbid group

The potential functional benefits of immunization with the combinational vaccine were further explored in vaccinated 3xTg mice from the premorbid group (Fig. 3a). AD mice immunized with either the single or dual vaccine before AD onset demonstrated recovery from muscular atrophy and exhibited improved performance compared to control mice (Fig. 3b). Notably, all vaccinated mice achieved performance levels in the hindlimb clamping test comparable to wild-type (WT) mice, likely reflecting the vaccines' effective mitigation of Tau pathology.

Subsequently, in the nest-building test, a sensitive indicator of hippocampal integrity, control mice receiving vector treatment were unable to fabricate intact nests. In contrast, nests built by mice from the dual vaccine group were successfully completed, achieving higher scores. Elevated mean nesting scores were also achieved by mice immunized with the Aβ and pTau vaccines alone compared to the control group, although statistical significance was not reached (Fig. 3c).

Moreover, the short-term memory of immunized mice was assessed through the novel object recognition test (NOR). 3xTg mice administered with the dual vaccine or Aβ single vaccine spent more time and showed a higher frequency of focusing on new objects compared to vector-treated mice (Fig. 3d and Supplementary Fig. 5b, c). In comparison, a slight but not significant increase in the exploration of novel stimuli was observed in mice inoculated with the pTau single vaccine. Collectively, these findings demonstrate that effective repair of hippocampal damage and rescue of short-term memory in 3xTg mice were induced by the dual vaccine.

Following this, the Morris water maze was employed to examine whether the dual vaccine positively impacts spatial learning and memory capacity (Supplementary Fig. 5d). In the hidden platform test, vector-treated 3xTg mice took a longer time to locate the platform compared to WT mice, indicating spatial learning deficits in 3xTg mice. Significantly, PP-based AD vaccines effectively reversed this spatial learning decline. Both the dual vaccine and Aβ vaccine-immunized mice exhibited a significantly shorter escape latency to the platform (Fig. 3e, f). In contrast, immunization with the pTau vaccine showed only a slight improvement in learning ability during the pre-training test. During the probe trial, which was performed subsequent to the removal of the hidden platform, mice that received the dual vaccine displayed a slightly improved performance compared to those immunized with a single vaccine, and their behavioral capacity was almost equivalent to that of wild-type (WT) mice. (Fig. 3g and Supplementary Fig. 5e). Moreover, dual vaccine-immunized mice demonstrated enhanced swimming speeds in the Morris water maze (Supplementary Fig. 5f), underscoring the beneficial effects of the combinational vaccine on memory and motor function in 3xTg mice. It is well known that sex plays a major role in the progression of AD[30], we also analyzed the therapeutic efficacy of dual vaccine in male and female 3xTg mice separately. The results of these behavioral assessments revealed that the cognitive abilities of both male and female AD mice were enhanced comparably following the administration of the dual vaccine, with no observed gender differences. Taken together, these findings, in conjunction with the pathology analysis results, robustly suggest that the dual vaccine simultaneously diminishes Aβ and Tau deposits in the brain, thus mitigating cognitive deficits in 3xTg mice.

Dual vaccine mitigates Aβ and pTau pathology and consequently relieves the behavior and cognitive deficits of mice from the onset cohort

The functional impact of the dual vaccine on 3xTg mice, administered after the onset of AD, was also further explored. Notably, Aβ plaque load was significantly reduced in the cortex of 3xTg mice immunized with both the single Aβ and the dual vaccine compared to control animals, with a relatively smaller difference observed in the hippocampal CA1 region (Fig. 4a, b). This diminution encompasses both soluble and insoluble forms of Aβ 42 in the brain homogenates of vaccinated mice (Fig. 4c, d). The combinational vaccine demonstrates enhanced clearance efficiency for both soluble Aβ 42 and insoluble Aβ plaques, even subsequent to disease onset, thereby emphasizing its potent therapeutic impact.

In terms of tau pathology, dual vaccine administration resulted in a noticeable decrease in neurofibrillary tangle (NFT) deposition across hippocampal and cortical areas (Fig. 4e, f and Supplementary Fig. 6a, b, e, f) and significantly lowered pTau protein levels as detected by the pTau396 antibody (Fig. 4g, h and Supplementary Fig. 6c, d, g, h). Consistently, the pTau single vaccine could also remove deposited NFT and soluble pTau protein in the AD mouse brain, but the degree of change was relatively lower than with the dual vaccine. In contrast to the mice in the premorbid cohort, the Aβ vaccine almost failed to diminish NFT and soluble pTau in the hippocampus of 3xTg mice from the onset cohort, potentially attributable to its restrained efficacy in mitigating hippocampal Aβ pathology.

Furthermore, the behavioral and cognitive abilities of 3xTg mice were analyzed when immunized after the onset of AD. In the hindlimb clamping experiment, the dual vaccine-treated mice exhibited a better therapeutic effect compared to the single vaccine and essentially reached the locomotor level of WT mice (Fig. 4i). Additionally, mice immunized with both single and dual vaccines showed an identical higher desire to explore a novel object, suggesting that the PP-based AD vaccine effectively improved the short-term cognitive ability of 3xTg mice (Fig. 4j). Moreover, in the MWM test, the latency time of each vaccinated group was shorter compared with the control group, albeit the difference did not reach a level of statistical significance (Fig. 4k and Supplementary Fig. 5i). Importantly, the dual vaccine-treated 3xTg mice exhibited a markedly increased platform crossing number compared to the single vaccines, indicating that the combination of Aβ and pTau vaccine exerts a more potent therapeutic effect on the cognitive decline in early AD mice (Fig. 4l).

Dual vaccine attenuates neuroinflammation to inhibit the progression of AD disease

Neuroinflammation, characterized by extensive gliosis and subsequent release of inflammatory cytokines, plays a vital role in the pathogenesis of

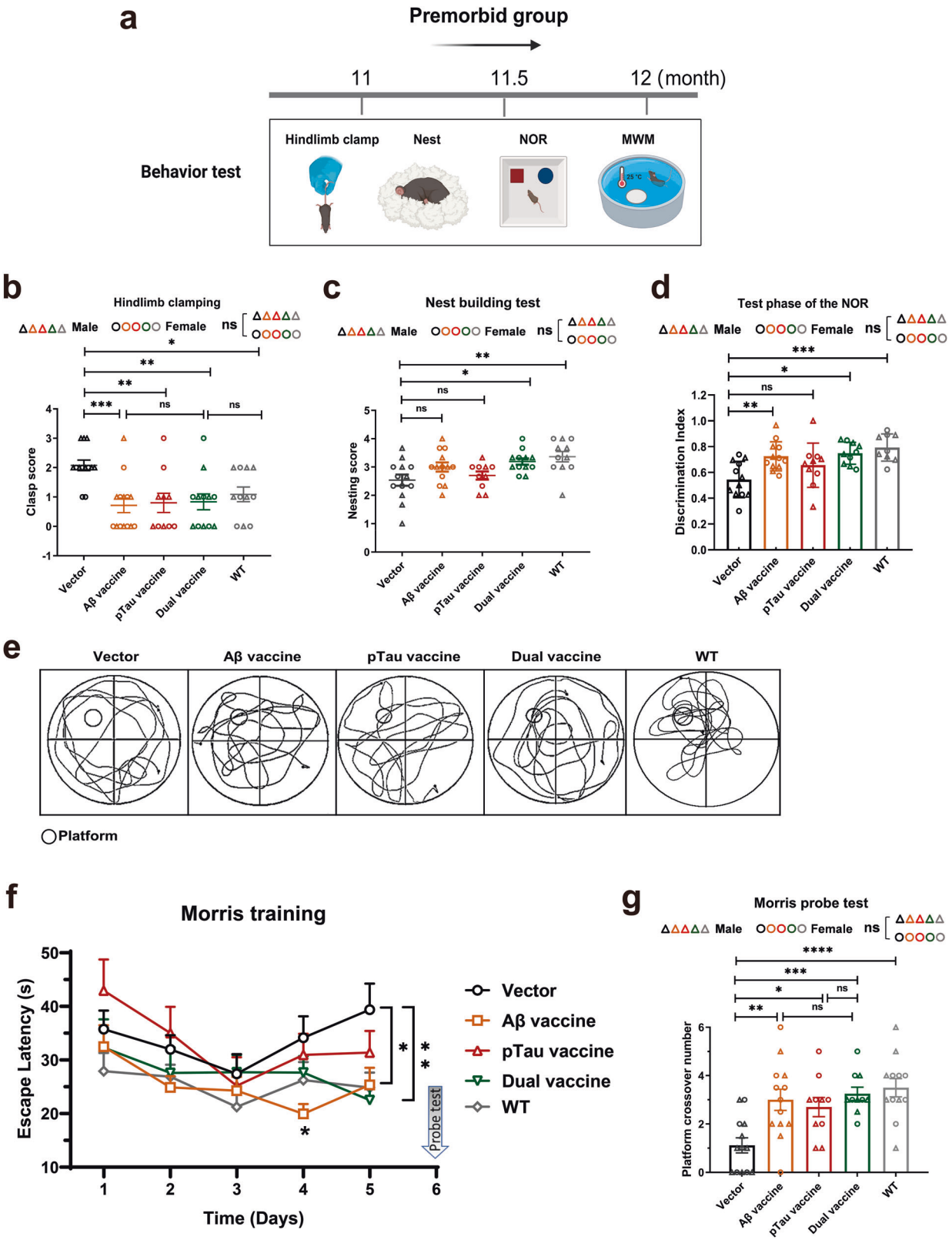

Fig. 3 | Impact of vaccines on behavioral and cognitive aspects in premorbid 3xTg mice. a Methods for behavioral evaluation: Description of the methods employed for evaluating the behavioral outcomes in mice post-vaccine treatment. **b** Hindlimb clamping (Clasp Score): Quantification of clasp scores in hindlimb clamping ($n = 10–13$ per group, one-way ANOVA). **c** Nest-building test: Scores from the nest-building test ($n = 10–13$ per group, one-way ANOVA). **d** Novel object recognition (NOR): Cognitive functions assessed through novel object recognition in mice ($n = 10–13$ per group, one-way ANOVA). **e** Morris water maze—probe trial: Representative track images of mice in the probe trial of Morris water maze. **f** Morris water maze—escape latency: Escape latency to the platform during the training trials in the Morris water maze ($n = 10–13$ per group, two-way ANOVA). **g** Morris water maze—platform crossings: Numbers of platform location crossings in the probe trial of Morris water maze ($n = 10–13$ per group, one-way ANOVA). *Data presented as mean ± SEM. Multivariate ANOVA was employed when $p \leq 0.05$. Bonferroni-corrected *t*-test was otherwise applied. Statistical significance denoted as $^{*}p < 0.05$, $^{**}p < 0.01$, $^{***}p < 0.001$; ns not significant. (Fig. 3a was created with BioRender.com).

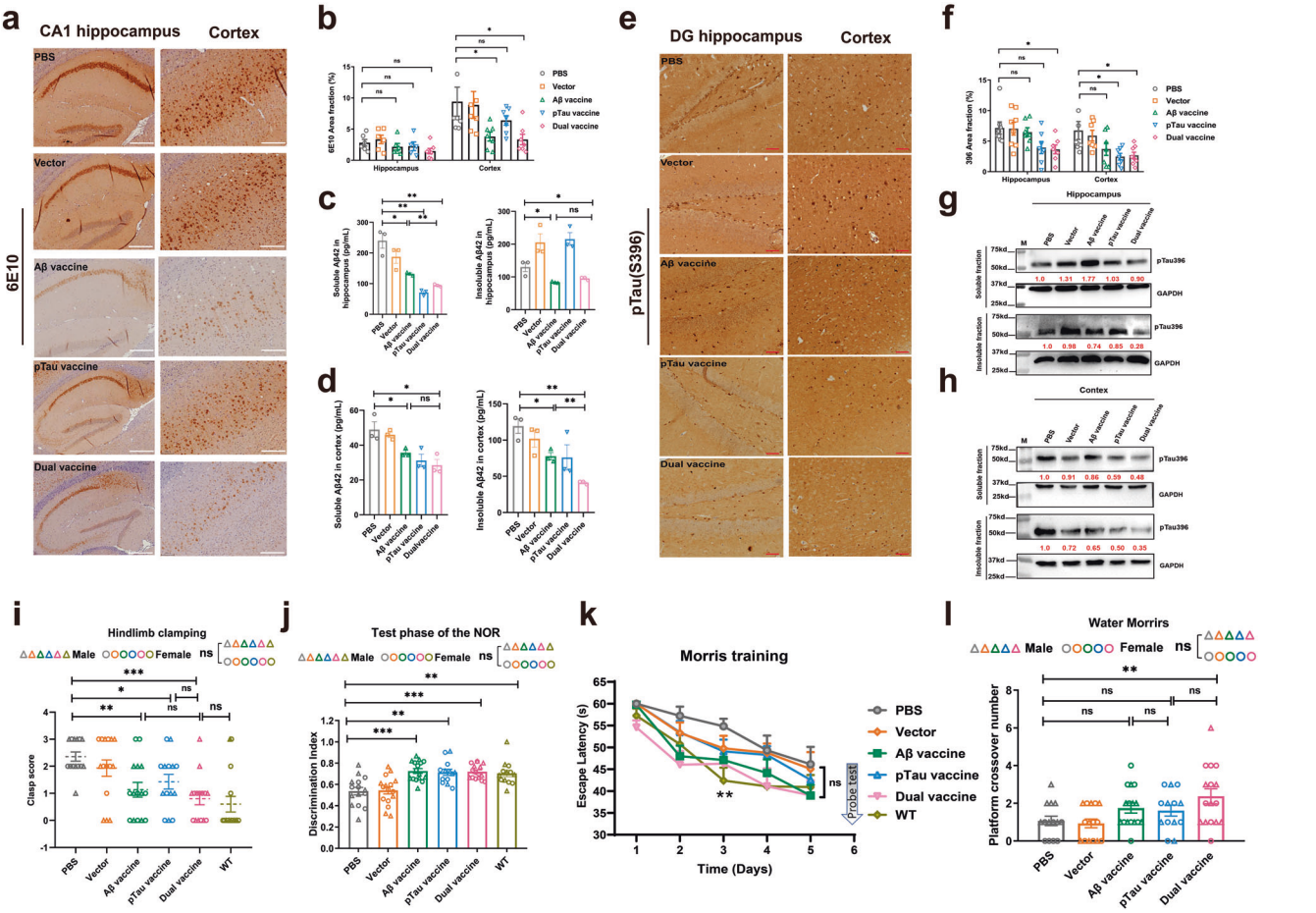

Fig. 4 | Impact of vaccines on pathological and cognitive parameters in onset 3xTg mice. a 6E10 immunostaining for Aβ burden: Immunostaining for Aβ burden in the brains of 3xTg mice treated with vaccines or vehicle. (White scale bar: 250 μm). **b** Quantification of Aβ immunostaining: quantification of 6E10 immunostaining in the hippocampus and cortex regions (n = 13–15). **c**, **d** Aβ42 analysis: Aβ42 levels in soluble and insoluble brain homogenates in the hippocampus. (**c**) and cortex regions (**d**) by flow cytometry (The experimental samples are mixed samples (n = 13–15) and repeated three times). **e** PHF-13 Immunostaining for pTau: Immunostaining for phosphorylated-tau (PHF-13) in the brains of 3xTg mice treated with vaccines or vehicle (Red scale bar: 50 μm). **f** Quantification of PHF-13 immunostaining: Quantification of PHF-13 immunostaining in the hippocampal DG and Cortex regions (n = 13–15). **g**, **h** pTau396 analysis: pTau396 levels in soluble and insoluble brain homogenates in the hippocampal DG (**g**) and Cortex regions (**h**) by western blot (n = 13–15). GAPDH served as the internal control. The relative content of each sample is marked with a red number. **i** Hindlimb clamping (Clasp Score): Clasp scores in hindlimb clamping (n = 13–15 per group, one-way ANOVA). **j** Novel object recognition (NOR): Cognitive functions assessed in novel object recognition (n = 13–15 per group, one-way ANOVA). **k** Morris water maze—escape latency: Escape latency to the platform during the training trials in the Morris water maze (n = 13–15 per group, two-way ANOVA). **l** Morris water maze—platform crossings: Numbers of platform location crossings in the probe trial of Morris water maze (n = 13–15 per group, one-way ANOVA). *Data were mean ± SEM. Multivariate ANOVA was employed when $p \le 0.05$. Bonferroni-corrected t-test was otherwise applied. *$p < 0.05$, **$p < 0.01$, ***$p < 0.001$; ns not significant.

AD[31]. In our study, we delved deeper into the effects of both single and dual immunotherapy on neuroinflammation in 3xTg mice. IHC analysis using an antibody against GFAP, an astrocyte marker, revealed that dual vaccine administration before the onset of AD significantly reduced astrogliosis in the brains of 3xTg mice compared with vector treatment (Fig. 5a). This reduction was notably more pronounced than that observed with the single vaccine, with the dual-vaccinated mice displaying a 50% decrease in the area positive for GFAP relative to vector-vaccinated mice (Fig. 5b).

Additionally, microglial activation, assessed by branching analysis and endpoint voxels analysis, was remarkably decreased in the hippocampus of dual vaccine-injected 3xTg mice compared with control mice (Fig. 5c–e). Consistently, WB analysis also showed reduced levels of GFAP and CD68 markers in the brains of dual vaccine-immunized mice (Fig. 5g, h). Importantly, while elevated levels of IL-1β and TNF-α were present in vector-treated 3xTg mice, the dual vaccine significantly reduced these proinflammatory cytokines, achieving a more pronounced decrease in TNF-α levels than the single vaccine (Fig. 5f).

Furthermore, in the onset cohort, the dual vaccine also potently decreased astrogliosis in the hippocampus of diseased 3xTg mice compared to the single vaccines (Supplementary Fig. 7a, b). Both the single and dual vaccine treatments increased the branching of microglia and repressed its activation in the mice brain (Supplementary Fig. 7c–e). Additionally, the levels of GFAP, CD68, IL-1β, and TNF-α significantly declined in the brains of 3xTg mice treated with the dual vaccine (Supplementary Fig. 7f–h).

Moreover, we also assessed for CAA-linked microhemorrhages following immunization using Perl's Prussian blue staining. The administration of the combinational vaccine did not result in an increase in antibody-induced microhemorrhages compared to the vector control group (Supplementary Fig. 8). In addition, no differences in the incidence of microhemorrhages were observed among the various vaccine treatment groups, suggesting the safety of this novel multi-targeting immunotherapy. Hence, these findings suggest that the combinational vaccine was able to relieve the aberrant inflammatory response in 3xTg mice, accompanied by the removal of Aβ and pTau pathology.

Potential functional mechanism of combinational vaccine-generated antibodies

To elucidate the potential mechanism underlying the amelioration of Aβ and tau pathology in 3xTg mice by the dual vaccine, we initially assessed the

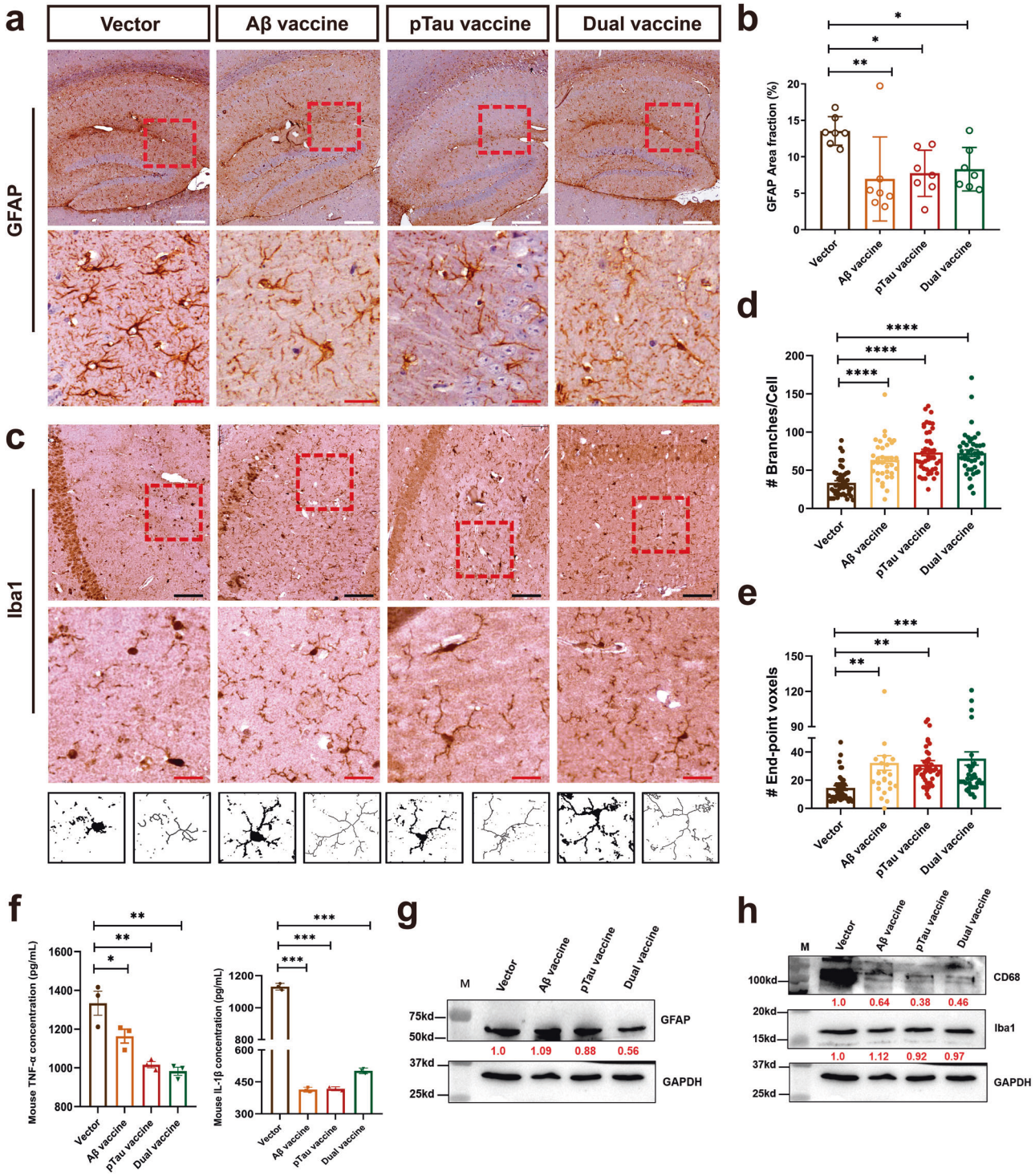

Fig. 5 | Dual vaccine reduces neuroinflammation in premorbid 3xTg mice. **a** GFAP immunostaining in the hippocampus of premorbid 3xTg mice treated with the dual vaccine or PP vehicle (Vector). (White scale bar: 250 μm, Red scale bar: 50 μm). **b** Quantification of GFAP immunostaining in the hippocampus. **c** Representative Iba-1 images and microglia quantification: Representative Iba-1 images and quantification of branching and endpoint of microglia in the hippocampus. $n = 7$ mice per genotype with 6–8 microglia quantified per mouse. (Black scale bar: 100 μm, Red scale bar: 50 μm) **d**, **e** Microglial morphology analysis: Quantitative assessment of branching (**d**) and endpoint (**e**) of microglia. **f** Cytokine levels in brain lysates: Levels of TNF-α (left) and IL-1β (right) in the brain lysates of 3xTg mice determined using corresponding ELISA kits. ($n = 6–7$). The experimental samples were mixed ($n = 6–7$) and repeated three times. **g**, **h** Western blot analysis: Western blot analysis of GFAP, Iba-1, and GAPDH in the brain lysates of 3xTg mice treated with the dual vaccine or vehicle. GAPDH served as the internal control. The relative content of each sample is marked with a red number. *Data presented as mean ± SEM. Multivariate ANOVA was employed when $p \le 0.05$. Bonferroni-corrected *t*-test was otherwise applied. Statistical significance denoted as $^{*}p < 0.05$, $^{**}p < 0.01$, $^{***}p < 0.001$; ns not significant.

levels of penetrating antibodies in the brain. The brain extracts of Aβ from the dual vaccine-immunized mice exhibited a relatively low Aβ antibody concentration, ranging from 0.5–1 ng/mL (Fig. 6a, b). In contrast, the levels of pTau antibody penetrating the brain were significantly higher than that of Aβ, ranging from 1–1.5 μg/mL, potentially due to elevated plasma pTau antibodies (Fig. 6a, b). Notably, the levels of cerebral antibodies in the brains of dual-vaccine-treated mice were lower than those from single vaccine-immunized mice (Fig. 6a, b). We hypothesized that the detected cerebral antibodies are tangle-free and non-functional antibodies and more brain-penetrating antibodies induced by the dual vaccine bound with Tau tangles. In line with this, serum Aβ42 levels reduced after dual vaccine treatment before the onset of disease, while remaining unchanged in the vector-treated group (Fig. 6c). This phenomenon did not appear in the onset group (Fig. 6d), suggesting that high-titer Aβ antibodies induced by the dual vaccine also bound to serum Aβ42, consequently facilitating its clearance.

Microglia plays important roles in clearing Aβ proteins through antibody-mediated Fcγ receptor-dependent phagocytosis. We found that microglia could colocalize with Aβ plaques in the brain of 3xTg mice after the immunization of single Aβ and dual vaccines (Supplementary Fig. 9). In addition, we performed an in vitro phagocytic assay by using BV2 cells and labeled Aβ oligomer. The results showed that purified Aβ antibody induced by the single Aβ and dual vaccines both significantly increased the uptake of Aβ oligomer in BV2 cells, indicating the involvement of microglia in the AD vaccine-induced antibody-mediated Aβ clearance (Supplementary Fig. 10a, b).

Subsequently, we purified polyclonal antibodies from the immunosera of all mice in both cohorts and analyzed their target engagement, specificity, and cytotoxicity protective function. Consistent with the clearance effect of Aβ and pTau pathology in vaccine-treated mice, antibodies produced by the Aβ vaccine recognized senile plaques in the brains of both APP/PS1 mice and 3xTg mice (Fig. 7a, b). Conversely, serum antibodies from pTau-vaccinated mice bound to tau tangles in the brain of 3xTg mice but were not sensitive to the amyloid plaques in APP/PS1 mice. Importantly, antibodies extracted from dual vaccine-treated mice recognized Aβ plaques in the brain of APP/PS1 mice as well as multiple pathological proteins in 3xTg mice brain (Fig. 7a, b). Dot blot assay results showed that antibodies produced by Aβ and dual vaccines recognized two species of toxic Aβ42, including Aβ oligomers and Aβ fibers, but showed no interaction with Aβ monomer (Fig. 7c and Supplementary Fig. 11a). Additionally, pTau antibodies induced by pTau single vaccine bound with pTau monomer and fibrils simultaneously (Fig. 7h and Supplementary Fig. 11c). In contrast, pTau antibodies purified from dual vaccine-immunized mice specifically recognized pTau fibrils but showed little recognition for the monomer, suggesting that the combination of two single vaccines triggers the induced antibody to be more specific for pathological Tau proteins (Fig. 7h). We also confirmed that the pTau antibody could not recognize Aβ species, and vise verse (Supplementary Fig. 11b, d).

Furthermore, thioflavin T (ThT) fluorescence assays assessing the impact of antibodies on Aβ or pTau aggregation showed that antibodies from Aβ- and dual vaccine-treated groups significantly reduced Aβ fibril populations quickly, with effectiveness increasing over time (Fig. 7d, e). Meanwhile, antibodies elicited by the pTau and dual vaccines in both age cohorts successfully repressed the assembly of pTau fibrils (Fig. 7i, j).

Finally, we examined whether the serum antibody of immunized mice could repress Aβ- or tau-mediated cytotoxicity in SH-SY5Y cells. As expected, the addition of 1 μM Aβ oligomers resulted in severe cell death to 55%, whereas serum antibodies stimulated by Aβ and dual vaccines significantly increased cell viability (Fig. 7f). Notably, the dual vaccine-elicited antibody mixture exhibited better protection against Aβ-induced cytotoxicity compared with the antibody produced by the Aβ solely vaccine. In the onset cohort, the purified antibody from vaccinated mice could only slightly protect the cell from Aβ toxicity, which might be due to the relatively lower levels of induced antibodies in the mice immunized after the AD onset (Fig. 7g). In addition, pTau antibodies purified from dual-vaccine treated mice also showed remarkably enhanced inhibition of pathological tau-induced toxicity in SH-SY5Y cells, presenting a greater extent than that from pTau single vaccine (Fig. 7k). Similarly, in the onset group, cell survival was moderately but significantly restored with the addition of pTau antibodies produced by the combinational vaccine (Fig. 7l). In summary, serum antibodies induced by the dual vaccine could specifically recognize various toxic forms of Aβ and pTau, inhibit the aggregation of pathological Aβ and pTau, and ultimately exert a protective effect on cytotoxicity.

Discussion

The predominant focus of Alzheimer's disease (AD) therapeutic strategies has been on targeting a single pathological mediator, yet these approaches have largely resulted in limited clinical improvement or have been associated with toxicity. This limitation has highlighted the ineffectiveness of single-target therapies in significantly slowing the progression of AD in patients, pointing to the potential need for combinational therapy that addresses multiple aspects of AD pathologies to achieve substantive disease modification. In the present study, we developed a dual vaccine utilizing PP (Noroviruses PP nanoparticles) targeting Aβ and pTau concurrently. Our findings revealed that the dual vaccine elicited robust and enduring antibody response against both Aβ and pTau. The resultant mixed antibodies significantly facilitated the removal of deposited senile plaques and neurofibrillary tangles (NFTs). Moreover, the vaccine effectively mitigates learning and memory deficits in the 3xTg AD mouse model. Notably, neuroinflammatory responses, including microgliosis, astrogliosis, and proinflammatory cytokines in the AD mouse brain, were markedly suppressed upon vaccination (Fig. 8).

Currently, the predominant focus of Alzheimer's disease (AD) immunotherapies is on the removal of pathological aggregates of either Aβ or tau. However, strategies that simultaneously target both molecules being seldom reported. In a pioneering effort, Davtyan H. et al. developed the first dual-targeting vaccine, a combination of two MultiTEP epitope vaccines targeting Aβ1–11 and tau2-18, respectively[32]. Consistent with our earlier findings, they observed that a dual-epitope vaccine expressing both Aβ and tau epitopes generated comparable levels of Aβ antibodies but significantly lower titers of tau antibodies. Both single and combinatorial vaccines generated elevated levels of antibodies specific to Aβ42 and/or tau2-18. Despite the promising initial results suggesting that a combined vaccination approach holds potential for inducing robust immune responses against both hallmark pathologies of AD, several critical questions remain unanswered: (1) The durability of antibody response in different mouse cohorts needs further investigation; (2) There is a crucial need for behavioral studies to determine whether these immune responses translate into cognitive improvement; (3) The efficacy of this combinational vaccine in preventing AD in bigenic mice, which carry both Aβ and tau pathologies, remains to be explored; (4) the impact of the dual vaccine which includes Aβ and a specific pathological pTau epitope, is still under study.

To further underscore the significance of a combinational vaccine in the preventive and therapeutic interventions for AD, we engineered a vaccine comprising Aβ1–6 and four phosphorylated Tau epitopes based on the Noroviruses PP nanoparticles platform. This platform includes multiple Th epitopes, which activate preexisting memory Th cells generated in response to norovirus infections, leading to a more robust and prolonged antibody response. Remarkably, prior to the onset of AD symptoms, the dual vaccine elicited robust and sustained Aβ and pTau antibody titers. It is noteworthy that the mean concentrations of antibodies induced by the PP-based dual vaccine were lower than those induced by the MultiTEP-based combinational vaccine. This discrepancy could be attributed to differences in antigen epitopes and immune response in two distinct bi-transgenic AD mouse models. Unlike the results reported by Davtyan H. in AD mice, our combinational vaccine induced a similar level of anti-Aβ antibodies but significantly higher titers of pTau antibodies than the single vaccine. We think that in the formulation of a dual vaccine, beyond the PP carrier of the pTau vaccine, the PP carrier protein of the Aβ vaccine could also provide Th epitopes to activate Th2 cells and further co-stimulate the pTau epitope-specific B cells. Nevertheless, the anti-Aβ antibody response induced by the

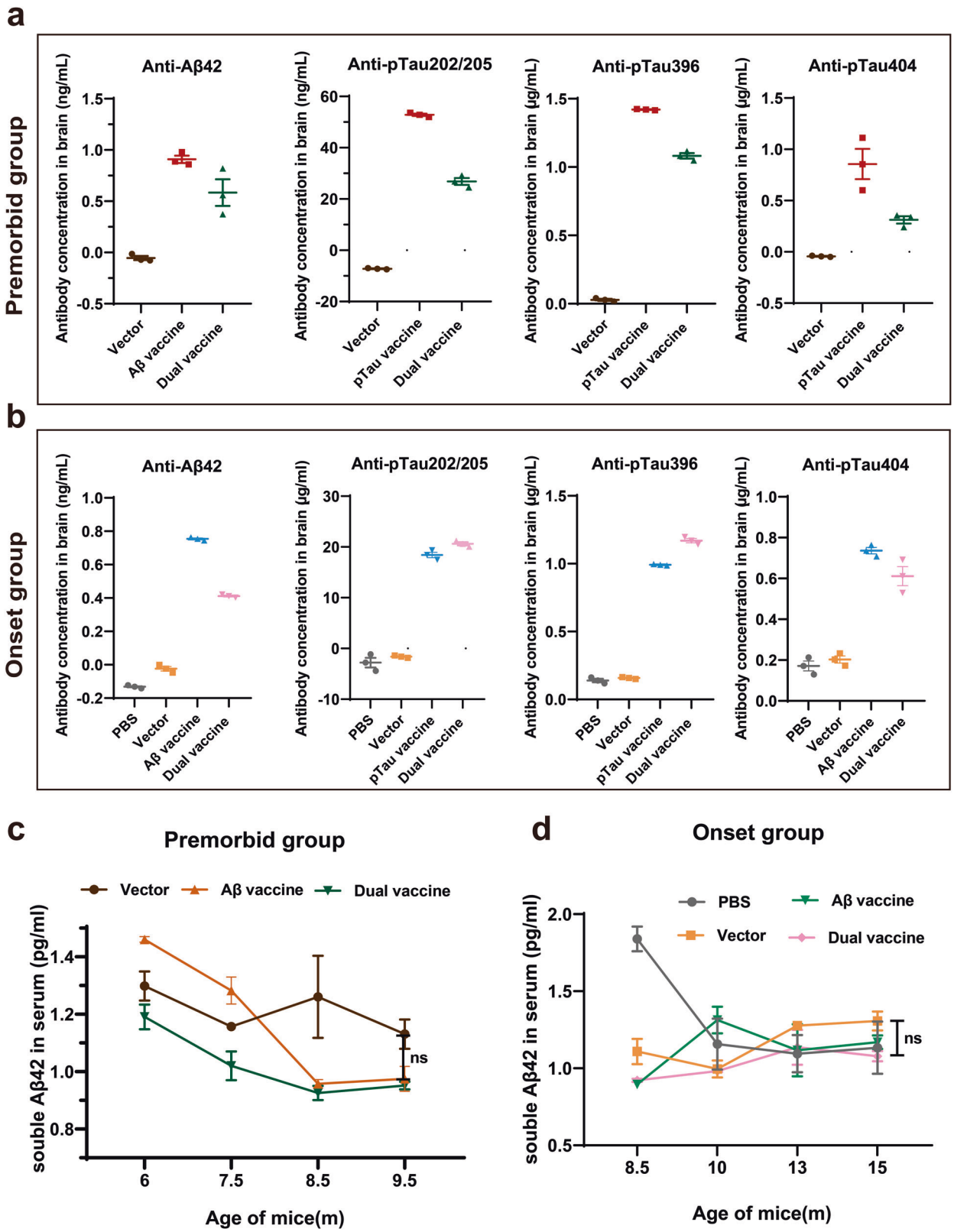

Fig. 6 | Potential functional mechanism of combinational vaccine-generated antibodies. a, **b** Antibody concentrations in the brain: Concentrations of antibodies against Aβ and individual phosphorylated Tau sites in the brain of 3xTg mice from the premorbid group (**a**) and onset group (**b**). **c**, **d** Vaccine-generated antibodies impact on Aβ42: Vaccine-generated antibodies entering the brain and altering the Aβ42 content in the brain and peripheral blood of mice after immunization in premorbid group (**c**) and onset group (**d**). *Data presented as mean ± SEM. Multivariate ANOVA was employed when $p \le 0.05$. Bonferroni-corrected *t*-test was otherwise applied. Statistical significance denoted as $^{*}p < 0.05$, $^{**}p < 0.01$, $^{***}p < 0.001$; ns not significant.

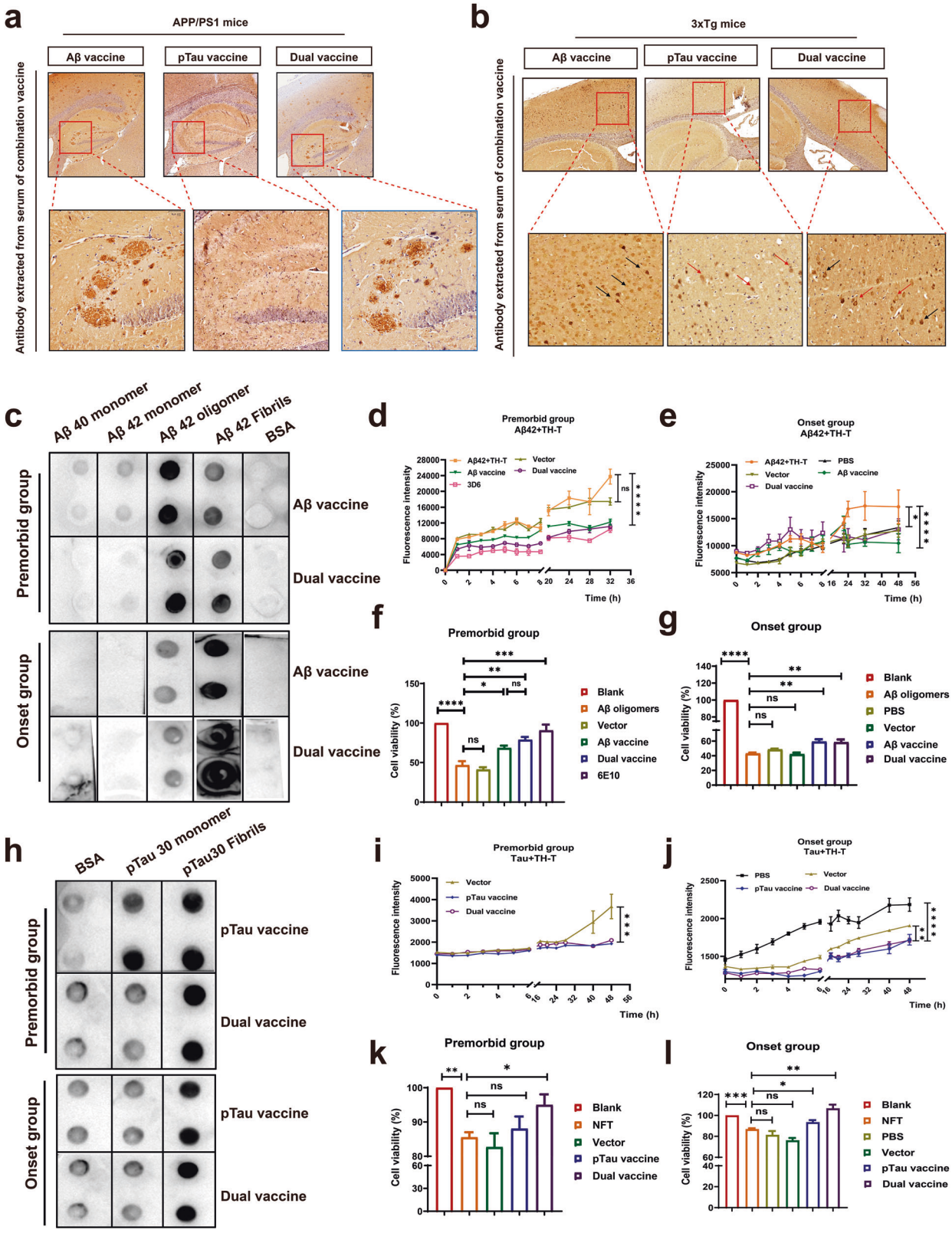

dual vaccine is similar to a single Aβ vaccine, indicating the differential immune response against Aβ and pTau antigens in AD mice. This suggests that the PP nanoparticle may be a more suitable platform for the development of a highly immunogenic dual-targeting vaccine for AD.

Concurrent with the increased titers of antibodies elicited by the combinational vaccine, noticeable neuropathological alterations were observed in the brains of mice treated with the dual vaccine in comparison to those treated with the single vaccine. This underscores the dual vaccine's capacity in mitigating two crucial pathological features of AD in 3xTg mice. Interestingly, a noteworthy decrease in tau pathology was observed in mice immunized with the Aβ single vaccine, and conversely, a reduction in Aβ pathology was observed in

Fig. 7 | Dual vaccine inhibits Aβ and tau aggregation, reduces Aβ oligomers, and tau tangles induced cytotoxicity. a, **b** Immunohistochemical staining on brain sections: Antibodies extracted from immunized serum used for immunohistochemical staining on the brain sections of untreated APP/PS1 mice (**a**) and 3xTg mice (**b**). (Serum dilutions 1:1000). **c** Recognition of various antigens and Aβ forms. The black arrow indicates Aβ plaques; The red arrow indicates tau tangles. Examination of the recognition of various antigens and different forms of Aβ by purified antibodies using dot blot. **d**, **e** Aβ aggregation kinetics: Assessment of the aggregation kinetics of 10 μM Aβ by thioflavin T fluorescence assay with or without serum antibodies. **f**, **g** Viability of SH-SY5Y cells (Aβ Oligomers): Determination of SH-SY5Y cell viability challenged with 25 μM Aβ oligomers in the presence or absence of 0.1 μM antibody purified from the serum after immunization. **h** Recognition of tau forms: Examination of the recognition of different forms of tau by purified antibodies using dot blot. **i**, **j** Tau aggregation kinetics: Assessment of the aggregation kinetics of 10 μM pTau by thioflavin T fluorescence assay with or without serum antibodies. **k**, **l** Viability of SH-SY5Y cells (Tau fibrils): Determination of SH-SY5Y cell viability challenged with 25 μM tau fibrils in the presence or absence of 0.1 μM antibody purified from the serum after immunization. *Data presented as mean ± SEM. Multivariate ANOVA was employed when $p \le 0.05$. Bonferroni-corrected *t*-test was otherwise applied. Statistical significance denoted as $^{*}p < 0.05$, $^{**}p < 0.01$, $^{***}p < 0.001$; ns not significant.

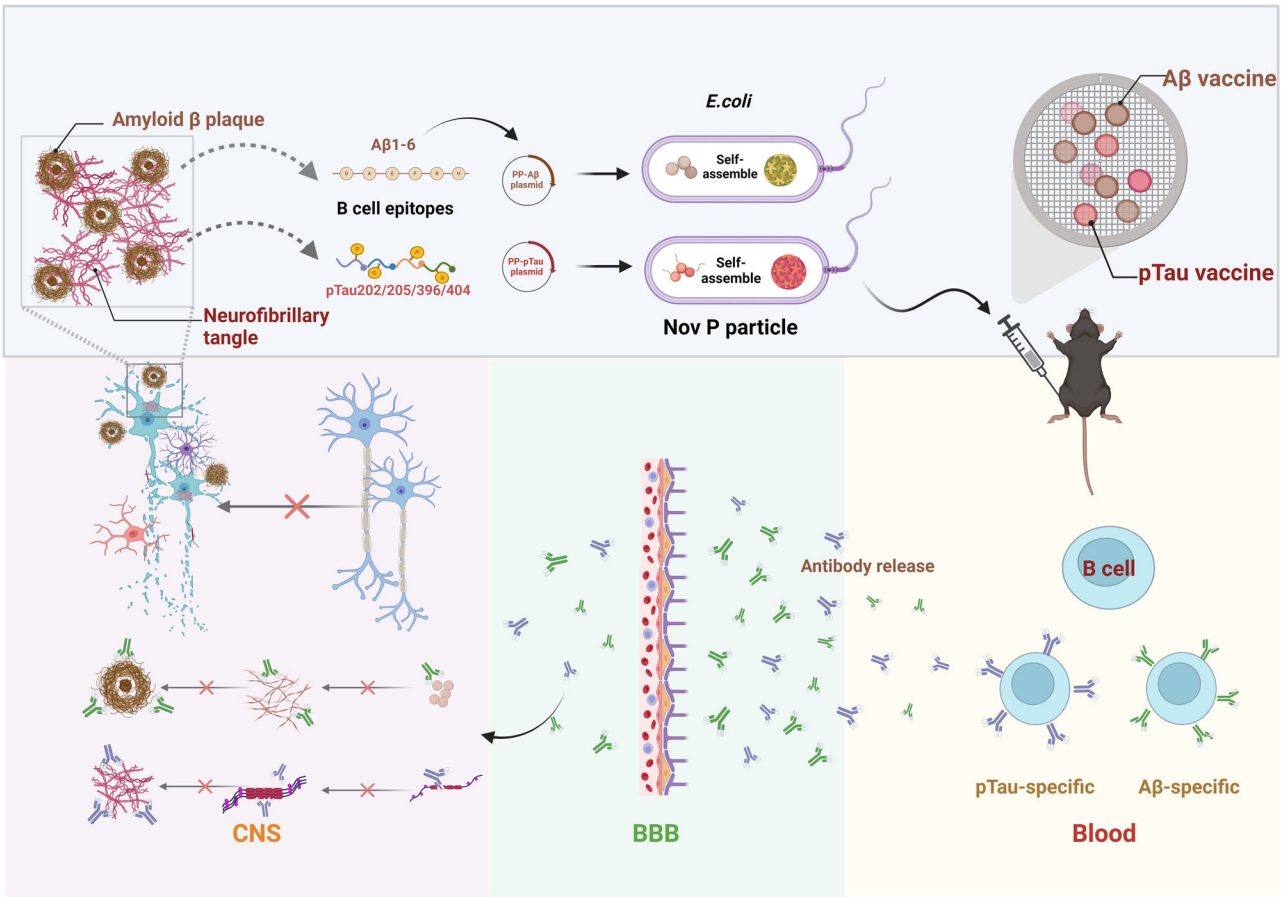

Fig. 8 | Design strategy and speculation on the mechanism of the dual vaccines. The dual vaccine elicited robust and enduring antibody response again both Aβ and pTau. Then, the resultant mixed antibodies significantly facilitated the removal of deposited senile plaques and neurofibrillary tangles, suppressed neuroinflammatory factors, and markedly enhanced cognitive abilities in 3xTg mice. (Created with BioRender.com).

those receiving the tau single vaccine, although to a lesser extent compared to the dual vaccine. This observation strongly supports the interplay between Aβ and tau pathology during the progression of AD. Similar to our observations, Davtyan H. et al. also found that significant reductions of several phosphorylated species of tau in mice immunized with the Aβ vaccine alone, and Tau vaccine could also slightly decrease the levels of soluble and insoluble Aβ in brain extracts[32]. Lecanemab, an FDA-approved Aβ antibody, could also improve downstream tau phosphorylation and slows Tau pathology in Temporal Lobe in mild AD patients[3]. In addition, Sigurdsson E. et al. demonstrated that the active immunization of pTau peptide could not only lead to the clearance of tau pathology but also of Aβ deposits in 3xTg mice[33]. Dai C. et al. also found that passive immunization with monoclonal tau antibody 43D leads to a sustained reduction in both Tau and Aβ pathologies in 3xTg mice[34]. Thus, the interplay between Aβ and pTau resulted in the mutual repression of Aβ or Tau pathology by the other vaccine treatment. This observation also potentially explains why the immunization with the combinational vaccine did not exert a distinctly superior influence on AD pathology compared to the single vaccine, highlighting the complexity of AD pathology and the potential benefits of a targeted dual approach.

Importantly, the reduction in pathological proteins following immunization was concomitant with the alleviation of neuroinflammation. Immunizing 3xTg mice with the dual vaccine, both before the onset of the disease and at its onset, significantly reduced microglial activation and astrogliosis. Moreover, treatment with the dual vaccine significantly decreased levels of proinflammatory cytokines, including IL-1β and TNF-α, in the mice brain. Furthermore, the combinational vaccine exhibited a greater reduction in activated astrocytes and TNF-α compared to the single vaccine. Thus, dual active immunotherapy effectively mitigated Aβ and pTau pathology while also curtailing detrimental neuroinflammation,

underscoring the therapeutic potential of targeting multiple AD pathologies simultaneously.

The impact of a dual-targeting AD vaccine on behavioral and cognitive improvement in the AD mouse model has remained largely elusive. In our study, the combinational vaccine notably ameliorated several behavioral deficits in 3xTg mice, such as reduced muscular tension and elevated learning and memory capacity. It's important to note that while we observed moderate differences in behavioral and cognitive analysis between dual-vaccine and single-vaccine treated mice, not all differences reached statistical significance. Those results suggested that the single vaccine effectively targeted its specific AD pathology while also alleviating pTau and neuroinflammation pathology. This multifaceted action led to significant improvements in clinical outcomes, which were nearly as effective as those observed in mice treated with the dual vaccine.

Given the complexity of AD pathophysiology and the irreversible nature of neurological damage, we designed both preventive and therapeutic approaches. Due to the high immunogenicity of the dual vaccine in the pre-onset cohort, the reduced levels of soluble and deposited Aβ and pTau proteins in vaccinated mice were much more pronounced than in mice treated after AD onset. Consistently, in the MWM analysis, immunized-premorbid mice exhibited the shortest latency in searching for the hidden platform and an increased dwelling time in the target quadrant compared to mice treated after onset, supporting the hypothesis that higher levels of induced antibodies are crucial for clearing AD pathology and enhancing cognitive function. Moreover, vaccination with the dual vaccine before the onset resulted in a more subdued neuroimmune response in the brain of 3xTg mice compared to those in the onset group. as evidenced by repressed microglia and astrocyte activation and fewer inflammatory factors. These results emphasize the early treatment before the severe AD pathology, which is crucial for enhancing learning and cognitive function.

The exact mechanism driving the antibody-mediated clearance of Alzheimer's disease (AD) pathology induced by vaccines remains to be fully understood. The direct-targeting mechanism suggests a small quantity of serum Aβ antibodies can traverse the blood–brain barrier (BBB), binding to pathological proteins, assisting in the clearance of extracellular Aβ through Fc-dependent microglia phagocytosis[35]. Serum pTau antibodies can also cross the BBB, are taken up by neurons through endocytosis, bind to the intracellular pathological tau proteins, and enable their clearance through lysosomal degradation[36–38]. However, the limited efficiency in detecting these antibodies within the brain, given the small percentage (0.1–0.2%) of IgG from the peripheral circulation that can cross the BBB, poses a significant challenge[39]. Notably, preclinical studies on the Aducanumab antibody indicated a mice brain penetration ratio of 1.3%, surpassing the 0.1% typical for systemically administered antibodies[40]. Conversely, Lecanemab displayed a low CSF antibody: serum antibody ratio in AD subjects, ranging from 0.13 to 0.29%[41]. In our investigation, we successfully detected Aβ and pTau antibody signals in AD mice brain homogenates, establishing a positive correlation between the level of antibody penetration and serum antibody concentration. This indicates that antibodies purified from the serum of immunized mice can specifically target and bind to pathological Aβ and pTau in the brain, preventing their aggregation in vitro and thereby validating the direct-targeting mechanism facilitated by the dual vaccine-induced antibody mixture. Furthermore, several studies demonstrated the "peripheral sink" hypothesis as an alternative mechanism of action for Aβ- or Tau-targeted immunotherapy[42]. Following dual vaccine treatment, soluble Aβ and pTau protein levels in 3xTg mice serum significantly decreased compared to the single vaccine and vector groups. This reduction was accompanied by a rapid decline in soluble and insoluble Aβ and pTau levels in the brain, indicating that the dual vaccine also functions through the "peripheral sink" pathway.

In conclusion, this combinational vaccine, simultaneously comprising Aβ and pTau vaccines, is an immunogenic and therapeutically potent solution. It successfully ameliorates multiple pathologies of AD and significantly enhances cognitive function in 3xTg mice. Nevertheless, so far, vaccines that use norovirus P particle as the platform have not yet been tested in human clinical trials. On one hand, the poor stability and heterogeneity of recombinant P particle made it unsuitable for the large-scale industrial production. On the other hand, noroviruses are the leading cause of acute viral gastroenteritis in human being, the preexisting antibody against the norovirus P particle may cause certain bad effects on the immunogenicity and efficiency of P particle-based vaccines. Thirdly, considering that the pS202/pT205 epitope was from the mid-region of Tau and pS396/pS404 was the C-terminal epitopes, this artificial combined pTau peptide might not be real and exert any physiological function in vivo. Thus, our findings underscore the need for further investigations into the efficacy of this multi-targeting AD vaccine in non-human primates and human subjects.

Methods

Mice

Eight-week-old female C57BL/6 wide-type mice were used for the immunogenicity analysis and 3xTg mice model were utilized for the evaluation of therapeutic effects of the vaccines. The 3xTg mice harboring PS1 M146V, APPswe, and Tau P301L transgenes were purchased from Laboratory animal origin and production license number Changzhou Cavens Biotechnology. All animals were reared in individually ventilated cages (IVC) in the Animal Experimental Platform, Core Facilities for Life Science, Jilin University. In a 12 h light/dark cycle with ad libitum access to food and water, Mice used in this study were not used for breeding and were reared by sex at a density of four to five mice per cage.

Epitope vaccine preparation—two recombinant proteins

The Aβ vaccine, named PP-3copy- Aβ1–6, is comprised of three copies of human Aβ1–6 inserted into three loops of the norovirus P particle. The exact amino acid sequence of the Aβ epitope is: GGGDAEFRHGGG-DAEFRHGGGDAEFRHGGG. For the generation of the Aβ vaccine recombinant plasmid, we used the engineered pET28a+ expression vector, which contains 6xhistidine on the C-terminal region of its polyclonal site to carry the coding sequence of Aβ vaccine protein. Subsequent purification of his-tagged Aβ vaccine protein involved the application of cell lysate supernatant to a HiSTrap FF chromatography column (GE Healthcare), followed by elution of the target protein using a linear imidazole gradient ranging from 50 mM to 300 mM. The Aβ vaccine protein was successfully eluted with 300 mM imidazole fraction. We have confirmed the existence of Aβ vaccine protein in that eluant by running SDS-PAGE gel and western blot analysis using anti-His antibody (Supplementary Fig. 1a, b). The particle size and TEM analysis also showed that Aβ vaccine protein could form the nanoparticles around 22 nm (Supplementary Fig. 1c, d).

For the generation of the pTau vaccine, we first used site-directed mutagenesis to replace the protruding amino acid of three loops of P protein with lysine (K) and named it as PP-3K carrier protein. Then the PP-3K particles were produced in Escherichia coli by Ni-NTA purification (Supplementary Fig. 1e–g). The target antigen, a phosphorylated Tau (pTau30) peptide, encompassing four phosphorylation sites (pS202/T205/S396/S404) of human Tau protein, was synthesized (GL Biochem) and modified to incorporate a C-terminal cysteine. The exact amino acid sequence and the four phosphorylation sites for pTau epitope is: sspgSpgTpgsrivykSpvvsgdtSprhlc (Capital letter means phosphorylated Tau site, represents pS202, pT205, pS396, and pS404, respectively). This pTau30 peptide was conjugated to the surface-exposed lysines of PP-3K (as indicated in the additional image) via the bifunctional crosslinker SMCC (Thermo Fisher Scientific, cat. no. 22360), with the conjugation efficiency confirmed through SDS-PAGE analysis. The size of the PP-3K carrier protein and pTau30 peptide is about 34 KD and 3 KD, respectively. After linking PP-3K and pTau30 by SMCC, the size of the main pTau vaccine protein product is 37 KD, which is equivalent to that one pTau30 peptide is attached to one PP-3K molecule. We also observed a small number of PP-pTau linkage products with 2 or 3 pTau peptides attached to the PP-3K carrier (Supplementary Fig. 1h, right panel, lane 2 and lane 3). In addition, since PP-3K protein itself contains lysine and cysteine, it is inevitable that pTau vaccine

will self-assemble into aggregates through SMCC linking system. Therefore, there are many pTau vaccine polymers ranging from 75 to 250 KD after connecting PP-3K with pTau30. Thus, if we combine the whole linkage products containing more than one pTau30 peptide, the linking efficiency of the pTau vaccine is about 50%.

Experimental protocols/vaccine immunization

Premorbid group: "In the premorbid phase, 3xTg mice, both male and female, were categorized into four cohorts. The groups received either Aβ vaccine (25 μg protein/dose, $n = 12$), pTau vaccine (25 μg protein/dose, $n = 10$), a combination of Aβ and pTau vaccines (25 μg + 25 μg protein/dose, $n = 12$), or the vector (PP particles) group (25 μg protein/dose, $n = 12$), each vaccine was formulated with CpG and MF59 adjuvant. Immunization commenced at 3–4 months of age with a bi-weekly intramuscular regimen for four doses, followed by booster doses at weeks 4 and 18 post-initial immunization. Serum samples were obtained prior to each immunization for anti-Aβ and anti-tau antibody assessment. At 11 months, after behavioral assessments were conducted, heart, liver, spleen, lung, kidney, and brain tissues were harvested following humane euthanasia.

Onset group, immunization was initiated at 6.5 months. This cohort included PBS ($n = 14$, 100 μL/dose), Vector ($n = 15$, 100 μL/dose, with CpG +MF59 adjuvant), Aβ vaccine ($n = 15$, 25 μg/dose, with CpG+MF59 adjuvant), pTau vaccine ($n = 14$, 25 μg/dose, with CpG+MF59 adjuvant), and dual vaccine groups ($n = 15$, 25 μg + 25 μg/dose, with CpG+MF59 adjuvant), maintaining a gender balance in each. Considering the temporal disparity in Tau and Aβ pathologies and the immunization frequency, a modified regimen was adopted. Concurrent immunization with Aβ and pTau vaccines was performed at 6, 6.5, and 7 months. However, the fourth and subsequent booster doses were administered separately: the Aβ vaccine at 7.5 and 9 months and the pTau vaccine at 8 and 10.5 months. Serum for antibody detection and inflammatory protein analysis was collected bi-weekly post-first immunization and continued until 13 months. Behavioral evaluations were conducted between 13.5 and 14.5 months, followed by humane euthanasia at 15 months for brain and organ harvest for homogenization and histopathological analysis.

All the experiments were performed in accordance with legal and institutional guidelines and were carried out under ethics, consent, and permissions of the Ethical Committee of Care and Use of Laboratory Animals at Jilin University (S2021065). Two weeks after the MWM test, the mice were deeply anesthetized with pentobarbital (100 mg/kg) and perfused with phosphate-buffered saline (PBS), followed by cervical dislocation. Animal experiments were performed in full compliance with the ARRIVE reporting guidelines[43].

Characterization of serum antibody response

The quantification of serum antibodies specific to Aβ and pTau30 was performed utilizing enzyme-linked immunosorbent assay (ELISA). ELISA plates, pre-coated with Aβ 1–42 peptide or pTau202/205-BSA, pTau396-BSA, and pTau404-BSA peptides (100 ng/well), facilitated this analysis. For calibration of Aβ antibody levels, mouse monoclonal antibody 6E10 (1:200 dilution, 803001, Biolegend, San Diego, CA, USA) was employed. Concurrently, antibodies targeting pTau202/205,396,404 were calibrated using AT8 (1:200 dilution, MN1020, Thermo Fisher Scientific, Waltham, MA, USA), PHF-13 (1:200 dilution, 829001, BioLegend, San Diego, CA, USA), and Phospho-Tau (Ser404) Polyclonal Antibody (1:200 dilution, 44–758 G, Thermo Fisher Scientific, Waltham, MA, USA), respectively.

Determination of the isotypic profile of vaccine-induced antibodies

The mouse monoclonal antibody isotyping reagent (Sigma-Aldrich, USA) was used to analyze the isotypes of antibodies generated against the vaccine.

Hindlimb clamping

Muscle atrophy in mice was assessed through the hindlimb clamping test. This involved suspending mice by their tails for 10 s while observing the contraction of their hind limbs. The contraction intensity was evaluated by three independent experimenters using pre-established scoring criteria, detailed in ref. 44.

Nest

Nest building, crucial for insulation, reproduction, and shelter in mice, was analyzed to understand complex physiological behaviors linked to various brain regions, including the hippocampus. Individual 3xTg mice were provided with 1.8 g of cotton (two 5 cm × 5 cm pieces) in a single cage, after changing the bedding material. Nest construction was evaluated by three trained experimenters 24 h later, using a scoring system ranging from 1 (no nest) to 4 (nearly perfect or perfect nest).

Novel object recognition task (NOR)

The NOR task, designed to assess learning and memory, comprises three phases: adaptation, training, and testing. During the adaptation phase, mice explored an object-free environment for 10 min, akin to the open field test. In the training phase, mice were exposed to two identical, odorless, and immovable objects. The testing phase, conducted an hour after the training, involved replacing one of the objects with a new one. The discrimination score for novel object exploration was calculated using the formula: (time exploring novel object/(time exploring novel object + time exploring familiar object)) × 100%.

Morris water maze test

The MWM test, a predominant behavioral experimental method in Alzheimer's disease (AD) research, evaluates spatial learning and memory in mice. The protocol involves an acquisition phase over five consecutive days, followed by a probe trial on the sixth day. The circular pool, sectioned into four quadrants and adorned with three distinct patterns on the walls, conceals a platform submerged 2 cm underwater in one quadrant. During the acquisition phase, mice, starting from different quadrants, navigate to find the hidden platform within 60–90 s, with the average latency across four daily trials recorded. On the probe trial day, with the platform removed, the subjects' spatial orientation is assessed by measuring the duration spent in the platform's quadrant and the frequency of crossing the former platform location.

Western blotting for detection of pathological proteins in brain homogenates

Pathologic examination of the brain and other organs. The mouse brains were separated into two hemispheres after removal. One hemisphere was deep-frozen in liquid nitrogen and homogenized, and further divided into reassembly buffer (RAB). Then 1 mL brain homogenate suspension was transferred to a 1.5 mL microfuge tube and centrifuged at 50,000×*g* for 20 min at 4 °C (Optima Max-XP, Beckman Coulter, Inc., CA). The pellet was resuspended with 1 mL RIPA buffer with protease and phosphatase inhibitor MIX and centrifuged at 50,000×*g* for 20 min at 4 °C to collect the supernatant as RIPA-soluble fraction (soluble fraction). The pellets were further disposed by 0.5 mL urea buffer (8 M urea and 5% (w/v) SDS, pH 7.2) at 2–8 °C overnight and centrifuged to separate the supernatant as urea-soluble fraction (insoluble fraction. The procedure details (the RAB and the RIPA solution formulations) are also described before[45,46]. The brain homogenate fraction samples of each mouse from the same group were mixed in a ratio of 1:1 before western blot analysis, which represents the average total Tau protein of pTau protein levels of the corresponding group. The other hemisphere was immersed in 4% paraformaldehyde for immunohistochemistry (IHC) to detect the levels of Aβ plaque, NFT, microglia, and astrocytes. The brain homogenates were used for western blot analysis, flow cytometry, ElisaKit, and the detection of inflammatory factors and chemokines by Elisakit.

For pathological examination of brain tissues, samples were homogenized in ice-cold RAB and RIPA buffers. Solution preparation methods are mentioned in the supplement. Western blot analysis involved resolving proteins on a 12% SDS-PAGE, followed by their transfer onto membranes

in transfer buffer, and overnight immunoblotting with phospho-tau (Ser202/Thr205) mAb (AT8, 1:1000 dilution, MN1020, Thermo Fisher Scientific, Waltham, MA, USA), Phospho-Tau (Ser396) mAb (PHF-13, 1:1000 dilution, 829001, BioLegend, San Diego, CA, USA), Phospho-Tau (Ser404) Polyclonal Antibody (1:1000 dilution, 44–758 G, Thermo Fisher Scientific, Waltham, MA, USA), GFAP mAb (1:1000 dilution, 2E1.E9, 644702, Biolegend, San Diego, CA, USA), Iba-1 mAb (1:1000 dilution, EPR16588, ab178846, Abcam, Cambridge, UK) or GAPDH mAb (1:1000 dilution, 60004-1-lg, Proteintech, Chicago, IL, USA). Subsequently, the membranes were incubated with Horseradish Peroxidase-conjugated AffiniPure Goat Anti-Mouse IgG (H + L) (1:10000 dilution, 111-035-144, Jackson ImmunoResearch, PA, USA) or Horseradish Peroxidase-conjugated AffiniPure Goat Anti-Rabbit IgG (H + L) (1:10,000 dilution, 111-035-003, Jackson ImmunoResearch, PA, USA) for 1 h at room temperature, and then treated with an enhanced chemiluminescence (ECL) solution for detection.

IHC (Immunohistochemistry)

For immunohistochemical analysis, brain sections underwent a gradient dewaxing process followed by antigen retrieval using citrate buffer. Post retrieval, sections were washed with TBST four times and sequentially treated with 3% hydrogen peroxide and 10% goat serum to block non-specific binding. The sections were then incubated with primary antibody overnight at 4 °C, including anti-β-amyloid 1–16 (1:400 dilution, 6E10, 803001, Biolegend, San Diego, CA, USA), Phospho-Tau (Ser202/Thr205) mAb (AT8, 1:100 dilution, MN1020, Thermo Fisher Scientific, Waltham, MA, USA), Phospho-Tau (Ser396) mAb (PHF-13, 1:500 dilution, 829001, BioLegend, San Diego, CA, USA), Phospho-Tau (Ser404) Polyclonal Antibody (1:300 dilution, 44-758G, Thermo Fisher Scientific, Waltham, MA, USA), GFAP mAb (1:500 dilution, 2E1.E9, 644702, Biolegend, San Diego, CA, USA), Iba-1 mAb (1:400 dilution, EPR16588, ab178846, Abcam, Cambridge, UK) and Anti-FOX3 (NeuN) mAb (1:500 dilution, 1B7, 834501, Biolegend, San Diego, CA, USA). Following primary antibody incubation, sections were washed and incubated with HRP-conjugated anti-mouse and rabbit secondary antibody polymers (abs996, absin) for 30 min at room temperature in the dark. Visualization was achieved using DAB chromogen, with incubation time adjusted based on color development. After drying, the slides were placed in a panoramic scanning image system for whole-slide scanning.

For standard image analysis of IHC images, including the determination of % area for antibodies such as 6E10, anti-pTau202/205, or anti-GFAP), TIFF image files were opened using ImageJ and converted to 8-bit greyscale files. Images displaying the minimum and maximum intensity of staining, along with representative samples from intermediate staining intensities, were utilized to establish an optimal threshold value. This threshold was determined by the investigator to accurately reflect the intended staining pattern across all experimental conditions within the cohort. That threshold was then held constant across all images in the cohort, and black and white images of selected regions of interest were generated and quantified as % area stained using the Analyze Particles function. At least 6 views per mouse per region were analyzed and averaged[46].

"Skeleton analysis" was used to measure the morphology of the microglia[47,48]. Isolating individual microglia in each image, then the images were skeletonized using the ImageJ skeletonize plugin. The particle analysis function was then used to remove background before using the Analyze Skeleton function in ImageJ to analyze the number of branches/endpoints per microglia cell.

Immunofluorescence

One series of the 30 μm sections was permeabilized, subjected to antigen retrieval, blocked, and then incubated with the following primary antibodies mouse anti-β-amyloid 1–16 (1:400 dilution, 6E10, 803001, Biolegend, San Diego, CA, USA) and rabbit anti-IBA1 (1:300 dilution, ab178846, Abcam, Cambridge, UK) at 4 °C for 24 h and followed by incubation with the corresponding fluorescent secondary antibodies at 37 °C for 2 h, including Alexa Fluor@555 Donkey pAb to Rabit IgG(1:400 dilution, ab150074, Abcam, Cambridge, UK) and DyLight-FITC goat anti-mouse IgG(1:400 dilution, IF-0091, Beijing, CHINA). Sections were stained with DAPI and sealed with an anti-fluorescence quencher.

Prussian blue

Paraffin sections were deparaffinized in a gradient for Prussian blue staining. A solution consisting of equal parts potassium ferrocyanide and hydrochloric acid was prepared to form the Prussian blue staining solution. Sections were immersed in this staining solution for one hour, followed by rinsing with distilled water. Subsequently, nuclei were stained with a nuclear fast red solution for 1 to 5 min, then washed under running water. Finally, the sections were dehydrated and mounted.

Determination of Aβ in brain and serum

The levels of Aβ42 in serum and brain homogenates (both soluble and insoluble fractions) of 3xTg mice were determined using Human Aβ42 ELISA kits (Uscn Life Science Inc., China), following the manufacturer's protocol."

Flow cytometry for detection of human Aβ40/42 and human tau

RAB and RIPA fraction of brain homogenates were applied for pathologic protein detection (Aβ40/42) with BioLegend LEGENDplex™ Human Neurodegenerative Biomarker Panel 1 (741197, BioLegend, USA). Briefly, the soluble and insoluble brain homogenate are mixed with beads and detection antibodies, and then analyzed by flow cytometer. We use the multi-factor online analysis software of biolegend to calculate the content of factors (Aβ42/Aβ40/Human Tau).

ElisaKit for detection of cytokine and chemokine

Plasma and soluble brain homogenate from mice were diluted twofold. All samples were tested using the following ELISA kits according to the manufacturer's instructions: TNF-α (Abcam, #ab252354), according to the manufacturer's instructions, IL-1β (Cloud-clone Corp, #SEA563Si96T) and IFN-α (Chenglin, #AD0081Mk).

Purification of serum antibodies from immunized mice

Serum antibodies from immunized mice were isolated using the saturated ammonium sulfate precipitation method, aiming for downstream in vitro validation. The procedure details are provided in the ref. 29.

Aβ oligomer and NFT preparation

Aβ oligomers were induced in vitro by dissolving 1 mg Aβ42 peptide in 110 μL of pre-cooled hexafluoroisopropanol (HFIP). Evaporate HFIP by placing it on ice with the lid open for 1−2 h. The resultant peptide film was dissolved in DMSO and then diluted with DMEM, followed by incubation at 4 °C for 24 h.

For the preparation of Aβ deposition, an initial Aβ reserve solution of 2 mM concentration was prepared. The Aβ 42 peptide was dissolved in 100 mM NaOH solution and subjected to sonication in a water bath for 30 seconds, thus forming the monomer reserve solution. To this solution, 10 mM Hepes, 100 mM NaCl, and 0.02% sodium azide were added to achieve a final concentration of 25 μM. The mixture was then incubated at room temperature for 21 days to facilitate Aβ deposition or tau fibrils.

To prepare tau fibrilization, the pTau30 peptide was prepared by dilution in a solution containing 10 mM 1,4-Dithiothreitol (DTT), 100 mM NaCl, and 10 mM HEPES, followed by a 1-h incubation at room temperature. Subsequently, heparin was added to achieve a final concentration of 8 mM. The mixture was then incubated with agitation at 37 °C for a period of 7 days. After incubation, the tau solution underwent centrifugation at 100,000×*g* for 1 h at 4 °C, resulting in a pellet comprised of aggregated tau[46]. This pellet was subjected to sonication at 65% power/amplitude for 30 s using a water bath sonicator, after which it was diluted for further use.

Aβ uptake assay

As previously described[49], FITC-labeled Aβ42 peptide was initially resuspended in 1% NH_4OH (10 μL), and then PBS was added to 1 mg/ml. The mixture was incubated at 37 °C for 12 h to promote Aβ42 oligomer. Following incubation, the mixture was diluted in DMEM/F12 medium to 5 μg/ml before it was applied to BV2 cells. After stimulation with 40 ng/ml IL-4 and 100 ng/ml dexamethasone for 24 h, cells were rinsed and incubated with FITC-labeled Aβ42 oligomer (5 μM) and serum antibodies (1 μM) in DMEM for 24 h. The cells were washed with PBS and fixed with 4% paraformaldehyde at room temperature for 15 min. Following this incubation, cells were washed with PBS and fixed with 4% paraformaldehyde at room temperature for 15 min. After fixation, cells underwent a final wash and were then treated with an anti-fluorescence quenching sealing solution containing DAPI at room temperature for 5 min. The uptake of Aβ42 oligomer was visualized using a CKX41-32PH automatic microscope (Olympus, Japan), and representative images were captured. The average signal intensity of Aβ42 oligomer in individual cells was quantified and expressed as a fold change relative to control cells, with at least 30 cells analyzed per experimental group.

Dot blot assay

A nitrocellulose membrane was pre-soaked in electroconversion buffer for 5 min before being placed in a dot blot apparatus. Protein samples, diluted to 10 μl, were applied onto the upper wells of the dot blot fixture. The membrane was then incubated in 5% skim milk powder for 30 min at room temperature with agitation. Antibody incubation and ECL detection were performed as described in the Western blot section.

CCK8

SH-SY5Y cells were cultured in 96-well plates, each well containing ~7500 cells in 100 μL of medium. The plates were incubated at 37 °C for 24 h to facilitate cell adhesion. Subsequently, 1 μM of either Aβ oligomers or tau fibrils, with or without antibodies purified from serum, were added to the cultures, followed by further incubation for 72 h at 37 °C. Cell viability was assessed by adding 10 μL cck8 to each well, incubating for 0.5 to 4 h at 37 °C, and measuring the absorbance at 450 nm using an enzyme-linked immunosorbent assay.

Th-T

Additional experiments were conducted to evaluate Aβ fibril formation in vitro using thioflavin T (Th-T) and to ascertain the inhibitory effect of antibodies on fibril formation. The procedure details are provided in ref. 28.

Statistical analysis

Statistical analysis was performed using GraphPad Prism 8.0 (GraphPad Software, Inc.) with a probability level set at 95%. Results are described as mean ± SEM. The relations among the measured data of behavioral or pathological monitoring at consecutive time points were analyzed using Mauchly's test of sphericity. Multivariate ANOVA was employed when $p \leq 0.05$. Bonferroni-corrected t-test was otherwise applied. Graphs were carried out using Adobe Illustrator 2020 and BioRender.com.

Data availability

All data upon which conclusions are drawn are included in the manuscript or in the supplemental information file provided.

Received: 4 February 2024; Accepted: 5 August 2024;
Published online: 20 August 2024

References

1. Scheltens, P. et al. Alzheimer's disease. *Lancet* **397**, 1577–1590 (2021).
2. Zhang, Y. et al. Amyloid β-based therapy for Alzheimer's disease: challenges, successes and future. *Signal Transduct. Target Ther.* **8**, 248 (2023).
3. van Dyck, C. H. et al. Lecanemab in early Alzheimer's disease. *N. Engl. J. Med.* **388**, 9–21 (2023).
4. Sims, J. R. et al. Donanemab in early symptomatic Alzheimer disease: the TRAILBLAZER-ALZ 2 randomized clinical trial. *JAMA* **330**, 512–527 (2023).
5. Usman, M. B. et al. Immunotherapy for Alzheimer's disease: current scenario and future perspectives. *J. Prev. Alzheimers Dis.* **8**, 534–551 (2021).
6. Jeremic, D., Jiménez-Díaz, L. & Navarro-López, J. D. Past, present and future of therapeutic strategies against amyloid-β peptides in Alzheimer's disease: a systematic review. *Ageing Res. Rev.* **72**, 101496 (2021).
7. Yu, H. J. et al. Safety, tolerability, immunogenicity, and efficacy of UB-311 in participants with mild Alzheimer's disease: a randomised, double-blind, placebo-controlled, phase 2a study. *EBioMedicine* **94**, 104665 (2023).
8. Hyman, B. T. et al. National Institute on Aging-Alzheimer's Association guidelines for the neuropathologic assessment of Alzheimer's disease. *Alzheimers Dement.* **8**, 1–13 (2012).
9. Ercan-Herbst, E. et al. A post-translational modification signature defines changes in soluble tau correlating with oligomerization in early stage Alzheimer's disease brain. *Acta Neuropathol. Commun.* **7**, 192 (2019).
10. Duka, V. et al. Identification of the sites of tau hyperphosphorylation and activation of tau kinases in synucleinopathies and Alzheimer's diseases. *PLoS ONE* **8**, e75025 (2013).
11. Bejanin, A. et al. Tau pathology and neurodegeneration contribute to cognitive impairment in Alzheimer's disease. *Brain* **140**, 3286–3300 (2017).
12. Imbimbo, B. P. et al. A critical appraisal of tau-targeting therapies for primary and secondary tauopathies. *Alzheimers Dement.* **18**, 1008–1037 (2022).
13. Ransohoff, R. M. How neuroinflammation contributes to neurodegeneration. *Science* **353**, 777–783 (2016).
14. Grubman, A. et al. Transcriptional signature in microglia associated with Aβ plaque phagocytosis. *Nat. Commun.* **12**, 3015 (2021).
15. Hickman, S. E., Allison, E. K. & El Khoury, J. Microglial dysfunction and defective beta-amyloid clearance pathways in aging Alzheimer's disease mice. *J. Neurosci.* **28**, 8354–8360 (2008).
16. Hopp, S. C. et al. The role of microglia in processing and spreading of bioactive tau seeds in Alzheimer's disease. *J. Neuroinflammation* **15**, 269 (2018).
17. Allen, N. J. & Lyons, D. A. Glia as architects of central nervous system formation and function. *Science* **362**, 181–185 (2018).
18. Hughes, C. et al. Beta amyloid aggregates induce sensitised TLR4 signalling causing long-term potentiation deficit and rat neuronal cell death. *Commun. Biol.* **3**, 79 (2020).
19. Zhao, J., O'Connor, T. & Vassar, R. The contribution of activated astrocytes to Aβ production: implications for Alzheimer's disease pathogenesis. *J. Neuroinflammation* **8**, 150 (2011).
20. Busche, M. A. & Hyman, B. T. Synergy between amyloid-β and tau in Alzheimer's disease. *Nat. Neurosci.* **23**, 1183–1193 (2020).
21. Hernandez, P. et al. Tau phosphorylation by cdk5 and Fyn in response to amyloid peptide Abeta (25–35): involvement of lipid rafts. *J. Alzheimers Dis.* **16**, 149–156 (2009).
22. Terwel, D. et al. Amyloid activates GSK-3beta to aggravate neuronal tauopathy in bigenic mice. *Am. J. Pathol.* **172**, 786–798 (2008).
23. Roberson, E. D. et al. Amyloid-β/Fyn-induced synaptic, network, and cognitive impairments depend on tau levels in multiple mouse models of Alzheimer's disease. *J. Neurosci.* **31**, 700–711 (2011).
24. Zhang, H. et al. Interaction between Aβ and tau in the pathogenesis of Alzheimer's disease. *Int. J. Biol. Sci.* **17**, 2181–2192 (2021).
25. Sperling, R. A. et al. The impact of amyloid-beta and tau on prospective cognitive decline in older individuals. *Ann. Neurol.* **85**, 181–193 (2019).
26. Hanseeuw, B. J. et al. Association of amyloid and tau with cognition in preclinical Alzheimer disease: a longitudinal study. *JAMA Neurol.* **76**, 915–924 (2019).

27. Timmers, M. et al. Relevance of the interplay between amyloid and tau for cognitive impairment in early Alzheimer's disease. *Neurobiol. Aging* **79**, 131–141 (2019).
28. Fu, L. et al. Norovirus P particle-based active Aβ immunotherapy elicits sufficient immunogenicity and improves cognitive capacity in a mouse model of Alzheimer's disease. *Sci. Rep.* **7**, 41041 (2017).
29. Sun, Y. et al. Norovirus P particle-based tau vaccine-generated phosphorylated tau antibodies markedly ameliorate tau pathology and improve behavioral deficits in mouse model of Alzheimer's disease. *Signal Transduct. Target. Ther.* **6**, 61 (2021).
30. Yan, Y. et al. X-linked ubiquitin-specific peptidase 11 increases tauopathy vulnerability in women. *Cell* **185**, 3913–3930.e19 (2022).
31. Leng, F. & Edison, P. Neuroinflammation and microglial activation in Alzheimer disease: where do we go from here? *Nat. Rev. Neurol.* **17**, 157–172 (2021).
32. Davtyan, H. et al. Testing a MultiTEP-based combination vaccine to reduce Aβ and tau pathology in Tau22/5xFAD bigenic mice. *Alzheimer's Res. Ther.* **11**, 107 (2019).
33. Rajamohamedsait, H. et al. Prophylactic active tau immunization leads to sustained reduction in both tau and amyloid-β pathologies in 3xTg mice. *Sci. Rep.* **7**, 17034 (2017).
34. Dai, C.-l et al. Tau passive immunization inhibits not only tau but also Aβ pathology. *Alzheimer's Res. Ther.* **9**, 1 (2017).
35. Davtyan, H. et al. Alzheimer's disease Advax(CpG)- adjuvanted MultiTEP-based dual and single vaccines induce high-titer antibodies against various forms of tau and Aβ pathological molecules. *Sci. Rep.* **6**, 28912 (2016).
36. Congdon, E. E. et al. Antibody uptake into neurons occurs primarily via clathrin-dependent Fcγ receptor endocytosis and is a prerequisite for acute tau protein clearance. *J. Biol. Chem.* **288**, 35452–35465 (2013).
37. Gu, J., Congdon, E. E. & Sigurdsson, E. M. Two novel Tau antibodies targeting the 396/404 region are primarily taken up by neurons and reduce Tau protein pathology. *J. Biol. Chem.* **288**, 33081–33095 (2013).
38. Krishnamurthy, P., Deng, Y. & Sigurdsson, E. M. Mechanistic studies of antibody-mediated clearance of tau aggregates using an ex vivo brain slice model. *Front. Psychiatry* **2**, 59 (2011).
39. Finke, J. M. & Banks, W. A. Modulators of IgG penetration through the blood-brain barrier: Implications for Alzheimer's disease immunotherapy. *Hum. Antibodies* **25**, 131–146 (2017).
40. Sevigny, J. et al. The antibody aducanumab reduces Aβ plaques in Alzheimer's disease. *Nature* **537**, 50–56 (2016).
41. Logovinsky, V. et al. Safety and tolerability of BAN2401-a clinical study in Alzheimer's disease with a protofibril selective Aβ antibody. *Alzheimers Res. Ther.* **8**, 14 (2016).
42. DeMattos, R. B. et al. Brain to plasma amyloid-beta efflux: a measure of brain amyloid burden in a mouse model of Alzheimer's disease. *Science* **295**, 2264–2267 (2002).
43. Kilkenny, C. et al. Improving bioscience research reporting: the ARRIVE guidelines for reporting animal research. *PLoS Biol.* **8**, e1000412 (2010).
44. Guyenet, S. J. et al. A simple composite phenotype scoring system for evaluating mouse models of cerebellar ataxia. *J. Vis. Exp*. 1787 (2010).
45. Sun, Y. et al. The behavioural and neuropathologic sexual dimorphism and absence of MIP-3α in tau P301S mouse model of Alzheimer's disease. *J. Neuroinflammation* **17**, 72 (2020).
46. Sheehan, P. W. et al. An astrocyte BMAL1-BAG3 axis protects against alpha-synuclein and tau pathology. *Neuron* **111**, 2383–2398.e7 (2023).
47. Young, K. & Morrison, H. Quantifying microglia morphology from photomicrographs of immunohistochemistry prepared tissue using imageJ. *J. Vis. Exp*. 57648 (2018).
48. Morrison, H. et al. Quantitative microglia analyses reveal diverse morphologic responses in the rat cortex after diffuse brain injury. *Sci. Rep.* **7**, 13211 (2017).
49. Chakrabarty, P. et al. IL-10 alters immunoproteostasis in APP mice, increasing plaque burden and worsening cognitive behavior. *Neuron* **85**, 519–533 (2015).

Acknowledgements

This work was supported by the National Natural Science Foundation of China [Grant No. 32070931 and 31971142], The Science and Technology Development Plan of Jilin province [20220508067RC], and the program of Lin Gang Laboratory [LG-GG-202401-ADA070200].

Author contributions

H.W. and W.K. conceived the project. H.W. and X.F. designed experiments and wrote the paper. X.F. conducted the majority of the experiments. Y.H., J.L., F.Y., M.D., M.C. and J.W. conducted some experiments. J.L., Z.L., D.S., Y.Z. and X.Y. provided wonderful suggestions for the progress of this study. All authors read and approved the final manuscript.

Competing interests

The authors declare no competing interests.

Additional information

Supplementary information The online version contains supplementary material available at https://doi.org/10.1038/s41541-024-00942-9.

Correspondence and requests for materials should be addressed to Wei Kong or Hui Wu.